Atmospheric Research 252 (2021) 105469

Contents lists available at ScienceDirect

Atmospheric Research

journal homepage: www.elsevier.com/locate/atmosres

Spatio-temporal distribution of the rainstorm in the east side of the Helan Mountain and the possible causes of its variability

Yuying Chen [a,b,c,*], Jianping Li [a,b,d], Xin Li [a,b], Suzhao Zhang [a,b,c], Yin Yang [a,b,c], Yang Su [a,b,c], Shanshan Yao [a,b,c], Jianhong Liu [a,b]

[a] Key Laboratory for Meteorological Disaster Monitoring and Early Warning and Risk Management of Characteristic Agriculture in Arid Regions, CMA, Yinchuan 750002, China
[b] Ningxia Key Laboratory of Meteorological Disaster Prevention and Mitigation, Yinchuan 750002, China
[c] Ningxia Meteorological Observatory, Yinchuan 750002, China
[d] Key Laboratory of Physical Oceanography, Institute for Advanced Ocean Studies, Qingdao National Laboratory for Marine Science and Technology, Ocean University of China, Qingdao 266100, China

ARTICLE INFO

Keywords:
Rainstorm
Spatio-temporal distribution
Topographic influence
Low-level jet
East side of the Helan Mountain

ABSTRACT

Compared with other arid areas, the convective rainstorm occurs more easily in the east side of the Helan Mountain, which is characterized by the short duration, large intensity, high precipitation efficiency and significant local distribution. In this paper, the 5-min and hourly precipitation at 512 regional automatic weather stations and other high-resolution observation data are used to analyze the spatio-temporal distribution and evolution characteristics of the rainstorm in the east side of the Helan Mountain during 2006 and 2019. Then, based on the daily precipitation data at 12 national observation stations, the rainstorm characteristics in this region during 1951 and 2005 are analyzed. On this basis, the rainstorm characteristics in the two periods are compared and studied. Finally, the possible causes of the distribution characteristics of rainstorm are initially discussed. The results show that the rainstorm with large magnitude and high intensity is mainly located in the mountainous region, and it mainly occurs in July with a high frequency period from afternoon to the first half of the night. Compared with 1951–2005, in 2006–2019 the rainstorm frequency, intensity and extremity are all increased, and the nocturnal and topographic features are more significant. The spatio-temporal distribution of rainstorm in the east side of the Helan Mountain is closely related to the nighttime enhancement of the low-level southeasterly jet and the interaction between the low-level jet and the mountainous topography. In the windward slope of the Helan Mountain, the interaction between the low-level jet and the mountainous topography could trigger or enhance the meso- and small-scale rainstorm systems, which would favor the occurrence of rainstorm. Overall, the conclusions in this study can deep the understanding of the rainstorms in the Helan Mountain, which could provide a reference for the monitoring and warning of rainstorms in this region.

1. Introduction

Under the background of global warming, the frequency of heavy rainfall events may increase in most of the land over the world (Li et al., 2011; Fischer and Knutti, 2015). This phenomenon has been confirmed in Europe, North America and Asia (Schmidli and Frei, 2005; Zhai et al., 2005; Jung et al., 2011; Nuissier et al., 2011; Chen and Zhai, 2013; Jing et al., 2016; Zhang et al., 2018). The eastern part of Northwest China (ENWC) is located in the innermost of the Eurasian continent. The long distance to the surrounding oceans could cause a more or less dry climate there. ENWC is one of the regions in China with the lowest annual precipitation (350 mm) and the lowest number of rainstorm days (less than 1d/a)(Ding et al., 2007; Shi et al., 2007; Yang et al., 2017); the east side of the Helan Mountain (37. 8°–39. 4°N, 105. 7°–107°E) is located in the north of the ENWC and the northern–central Ningxia Province. The annual precipitation is less than 200 mm, which is the driest area in ENWC. However, the observation facts over the last decade show that although the number of rainfall days in the ENWC has decreased, both the number of rainstorm days and the rainfall intensity have increased (Xu et al., 2011; Li et al., 2013; Chen et al., 2014; Deng

* Corresponding author at: Key Laboratory for Meteorological Disaster Monitoring and Early Warning and Risk Management of Characteristic Agriculture in Arid Regions, CMA, Yinchuan 750002, China.
E-mail address: chenyuy@sina.com (Y. Chen).

https://doi.org/10.1016/j.atmosres.2021.105469
Received 15 July 2020; Received in revised form 23 November 2020; Accepted 10 January 2021
Available online 11 January 2021

et al., 2014; Qin et al., 2017; Wang et al., 2003). In the recent past, the number of rainstorm days in the east side of the Helan Mountain tends to be anomalously frequent, and meanwhile the amount and intensity of rainfall also keep on setting new historical records (Chen et al., 2018; Sun et al., 2018). For example, at the night of August 21, 2016 and the night of July 22, 2018, the 12 h rainfall in the Huaxuechang reached 241.7 mm and 277.6 mm, respectively, which are the only two processes of extraordinary rainstorm of more than 200 mm since the meteorological records in Ningxia Province. The rainstorm triggered mountain torrents in many places, which affected many cities or counties causing the death of four people. As a result, the economic loss reached nearly 400 million yuan. Although the amount and intensity of these two rainfall processes are only about 50% and 20% of the extreme rainstorm in South and North China, the precipitation efficiency is higher than that in North China and is close to that in South China. The relative intensity of the rainstorm is more intense than that of South China and North China (Chen et al., 2017a, 2017b). It can be seen that although the probability of rainstorm in the east side of the Helan Mountain is low, the intensity and efficiency of precipitation are high. In addition, the geological and ecological environment is fragile due to the drought all year round. Once rainstorm occurs, it will cause serious losses.

Most of the climate statistics of rainstorm in China are based on observed daily precipitation which is obtained from national observation stations. The reasons are as follows. First, the data sequences of national stations are long, high-quality and well-managed; second, regional automatic weather stations (regional stations) are lately constructed, widely distributed, difficult to manage, relatively poor in quality and have different lengths of data sequences; third, traditional global or regional climate models have limited ability in simulating the physical processes of extreme precipitation at the sub-daily scale (Hanel and Buishand, 2010; Ban et al., 2014), which is difficult to be captured based on conventional meteorological observations from national stations. Before 2006, there were only twelve national stations in the east side of the Helan Mountain, with two in mountainous areas. However, with the deployment of intensified network of automatic weather station in the recent decades, the number of station has increased to 512 by the end of 2019, with 78 additions in mountainous areas. The spatial resolution has been improved from hundreds of kilometers to about 5 km, and the temporal resolution has also increased from 3 to 6 h to 5 min.

Although rainstorm occurs under the interactions of different scale weather systems, it is a mesoscale phenomenon (Johnson and Mapes, 2003; Ray, 1986; Tao and Ding, 1981; Tao, 1980). So, conventional meteorological observations are often difficult to capture it, and the previous climatic statistics cannot detailedly reflect the mesoscale distribution characteristics and topographic effects of rainstorm. At the same time, due to the uncertainties of initial conditions and the physical-process parameterization, the current operational numerical models have limited ability to simulate precipitation over complex terrain (Chen et al., 2018; Xue, 2005). Due to the limitations of observation accuracy, numerical simulation ability and scientific understanding, forecasters have insufficient understanding of the formation mechanism of rainstorms triggered by the topography and the low-level jet (LLJ), leading to the frequent false forecast of the rainstorm events (Chen et al., 2020; Tao, 1977). Therefore, it poses many problems and challenges to the rainstorm-disaster prevention and mitigation. Although the observational data with high spatio-temporal resolution is only in a few decades, it is enough to question and correct the previous climatic statistics of rainstorms. Moreover, the relative study can better reveal the triggering and enhancing effects of topography on the mesoscale rainstorms at the eastern foot of the Helan Mountain.

Aiming at the above shortcomings, this study focuses on the mesoscale rainstorm, and makes full use of the high resolution meteorological observation data. Then, the variation of extreme value, the distribution of rainstorm center, the frequency, the concentration time and area are statistically analyzed, so as to reveal the distribution and variation characteristics of the orographic rainstorm. Overall, this study could provide more statistics of the orographic rainstorm. On this basis, the jointly effect of the LLJ and the topography on rainstorms is preliminary discussed. The results in this study could improve the understanding on the formation mechanisms of orographic rainstorms in arid areas, and could enhance the disaster prevention and mitigation ability on flash floods in arid areas. The remainder of this paper is organized as follows. Section 2 gives the data and method. The spatio-temporal distribution characteristics of rainstorms in the east side of the Helan Mountain are presented in section 3. Section 4 preliminary explores the joint impact of the LLJ and topography on the distribution of rainstorms. Conclusions and discussion are given in section 5.

2. Data and method

In this paper, the east side of the Helan Mountain is selected as the study area. Then, based on the high-resolution rainstorm dataset, the climate statistics, the synoptic analysis method and the thermal-dynamic diagnosis method, the spatio-temporal characteristics of rainstorms and the influence of LLJ and topography on the distribution of rainstorms are investigated detailedly. The technical route is shown in Fig. 1, and the specific four steps are shown in the following four subsections.

2.1. Establishment of the rainstorm dataset

The rainstorm dataset is consisted of four types of data: the conventional and non-conventional observation data, the model reanalysis data and the surface intensified observation data. The specific information of the four types of data is given in Table 1. The topographical distribution of the study area is presented in Fig. 2. The region with the altitude above 1200 m is the Helan Mountain area, and the region with the altitude lower than 1200 m is the Yinchuan Plain. The time in this paper denotes the Beijing time.

The 5-min and hourly precipitation data is from 512 observation stations, the spatial resolution is 5–8 km, and the data period is from 2006 to 2019. The distribution of the stations is shown in Fig. 2a, in which there are 146 mountain stations and 366 plain stations. The lightning data is from 2007 to 2019, and the spatial and temporal resolutions are 500 m and 1 ms, respectively. The lightning identification in 2006 is based on the weather phenomenon observation at national stations. The 6-min radar data is from the C band radar in Yinchuan (38.47°E, 106.2°N) with the elevation of 1111.6 m, and the data period is from 2006 to 2019. The 6-h ERA-interim daily data ($0.125^\circ \times 0.125^\circ$) is also from 2006 to 2019, and the data include the surface pressure and other six elements in 13 vertical levels (875–300 hPa), which are temperature, u and v components of wind, vertical velocity, relative humidity and specific humidity. The daily precipitation is obtained from 12 national observation stations, and the data period is from 1951 to 2005. The distribution of the 12 stations is shown in Fig. 2b, in which there are 2 mountain stations and 10 plain stations.

2.2. Spatio-temporal distribution and variation characteristics of rainstorms in the east side of the Helan Mountain

According to the Fifth Assessment Report of Intergovernmental Panel on Climate Change (IPCC, 2013) and the precipitation classification standard of China Meteorological Administration (2012), the conventional characteristic quantities, such as rainstorm day, frequency and extreme value, are analyzed. Combined with the researches of Orsolini et al. (2015), Tu et al. (2011), Xu and Wang (1986) and Bai et al. (1988), the characteristic quantities that can reflect the rainstorm characteristics in the northwest arid areas, such as the precipitation efficiency and relative intensity, are introduced. The definition and standard of each characteristic quality are as follows:

For rainstorm and rainstorm day, the statistical period is from 20:00 of the previous day to 20:00 of the current day. When the 24-h

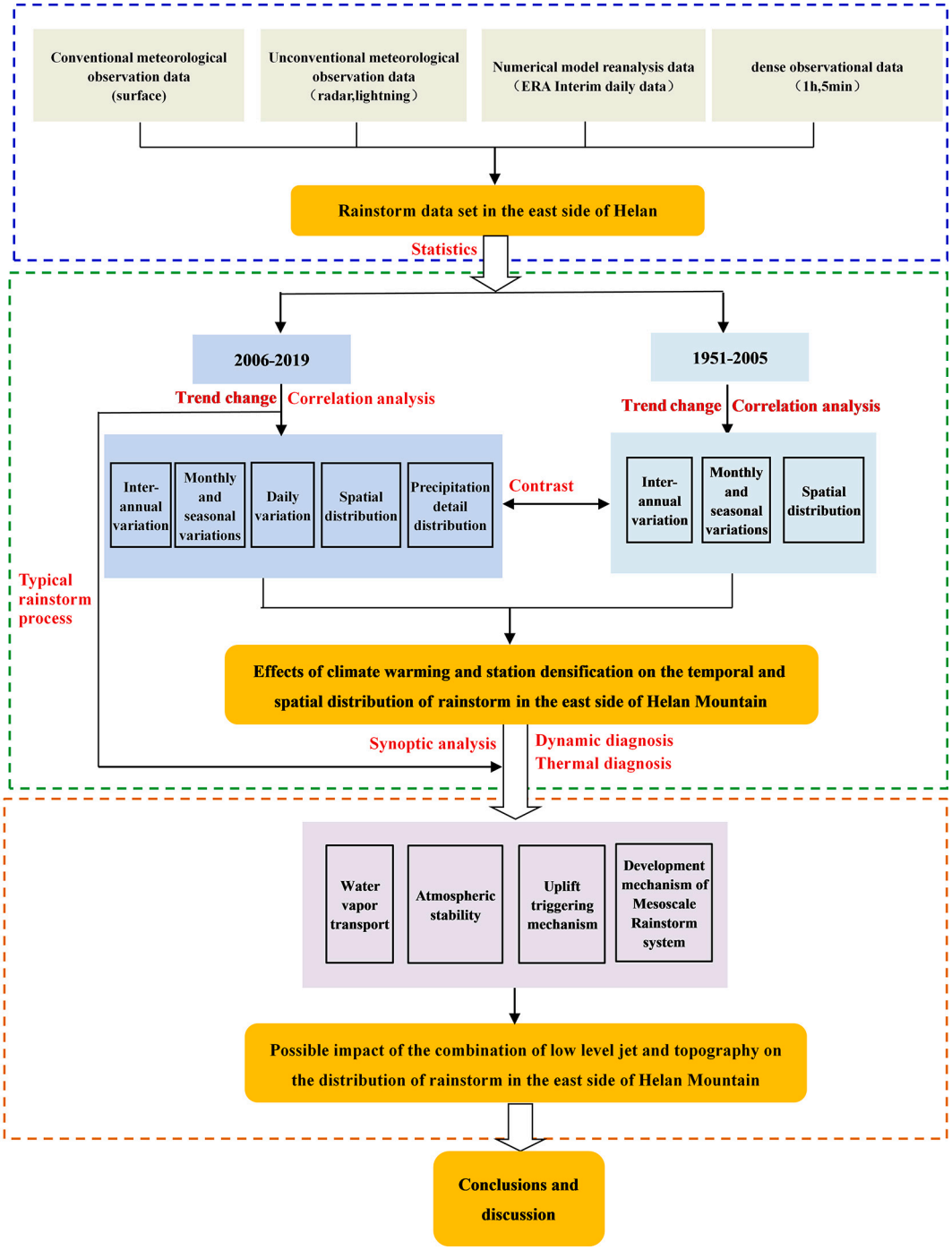

Fig. 1. Research method roadmap.

precipitation (R_{24}) $\geq$ 50 mm, it is defined as a rainstorm event. If rainstorm occurs in any station of the study area, it is recorded as a rainstorm day. Specifically, when 50 mm $\leq R_{24} <$ 100 mm, it is defined as general rainstorm (GR); when 100 mm $\leq R_{24} <$ 200 mm, it is defined as heavy rainstorm (HR); when $R_{24} \geq$ 200 mm, it is defined as extraordinary rainstorm (ER). Similarly, the short-time rainstorm is defined and classified as follows. With the 1-h precipitation recorded as R_{1h}, when 20mm $\leq R_{1h} <$ 40mm, it is defined as general short-time rainstorm; when 40mm $\leq R_{1h} <$ 60mm, it is defined as heavy short-time rainstorm (HSR); when $R_{1h} \geq$ 60 mm, it is defined as extraordinary short-time rainstorm (ESR).

Then, the precipitation efficiency and the relative intensity are defined as follows.

$$\text{Precipitation efficiency } (P_{1h}) : P_{1h} = \frac{R_{1h}}{R_{24}} \quad (1)$$

$$\text{Relative intensity } (F) : F = \frac{R_{24}}{R_{ave}} \quad (2)$$

In Eqs. 1 and 2, R_{1h} and R_{24} respectively correspond to 1-h and 24-h rainfall. R_{ave} at national observation stations is the 30-year (1981–2010) average of annual precipitation, while R_{ave} at regional observation stations is the annual precipitation averaged since the complete meteorological observations are available.

In order to highlight the extreme and catastrophic characteristics of rainstorm in arid areas, the rainstorm process is defined. Referring to the

Table 1
Rainstorm data set in the east side of the Helan Mountain.

Time	Data Type	Data Source	Level	Parameter	Temporal Resolution	Spatial Resolution
2006–2019	dense observation	Ningxia Meteorological Information Center	/	precipitation	5 min,1 h	5-8 km
	Yinchuan C-band Doppler weather radar		0.5°,1.5°,2.4°,3.4°,4.3°,6.0°,9.9°, 14.6°,19.5°	echo intensity, velocity, top height, vertical integrated liquid water content	6 min	5 cm
	ERA5 hourly data	European Centre for Medium-Range Weather Forecasts reanalysis data	875 hPa,850 hPa,800 hPa,750 hPa, 700 hPa,650 hPa,600 hPa,550 hPa, 500 hPa,450 hPa,400 hPa, 350 hPa,300 hPa	Pressure, Temperature, U and V component of wind, Vertical velocity, relative humidity, Specific humidity	6 h	0.125° × 0.125°
2007–2019	thunder and lightning	Ningxia Meteorological Information Center	/	lightning	1 ms	500 m
2006	thunder and lightning		/	lightning	3 h	50–100 km
1951–2005	conventional meteorological observation		/	precipitation	24 h	50–100 km

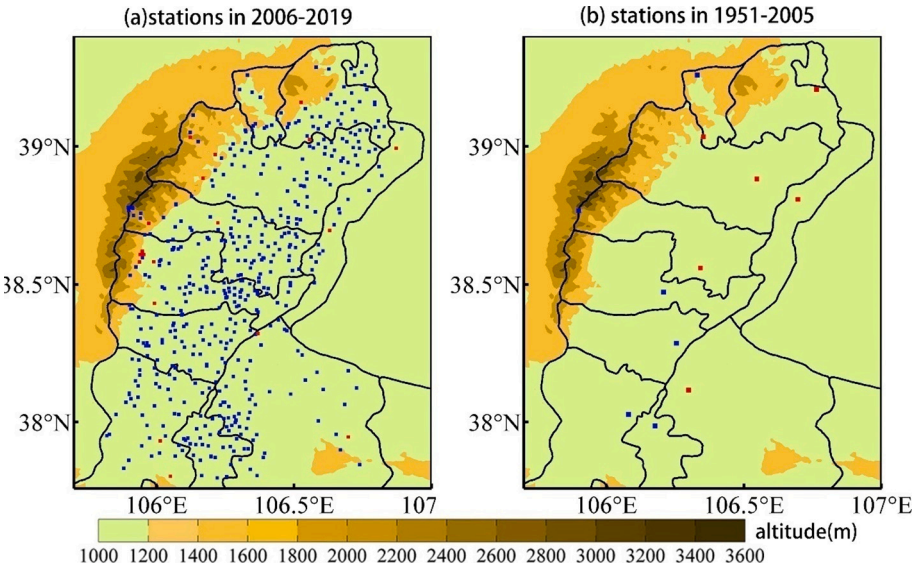

Fig. 2. Topography of the east side of the Helan Mountain and the distribution of weather stations (red and blue dots) in (a) 2006–2019 and (b) 1951–2005. Shading indicates the altitude (unit: m). Red dots indicate the precipitation centers during rainstorm processes.

past studies (Chen et al., 2020; Yao et al., 2017; Shao et al., 2015; Chen et al., 2008), before 2006 when $R_{24} \geq 50$ mm occurs at two or more adjacent stations, it is defined as a rainstorm process. After 2006, when the 24-h cumulative rainfall (R_{24}') ≥ 100 mm occurs at one or more stations, it is defined as a rainstorm process; otherwise when $R_{24}' \geq 25$ mm occurs at five or more adjacent stations, in which $R_{24}' \geq 50$ mm occurs at three or more adjacent stations, it is also defined as a rainstorm process. The time when there are at least five stations with $R_{1h} \geq 2$ mm is regarded as the beginning of the process; when there is no precipitation for three consecutive hours, it is considered as the end time of the process, and if the duration of rainfall exceeds 24 h, the time when there is no more than five adjacent stations with $R_{1h} \leq 2$ mm is considered as the end time. According to the regional average rainfall $\left(\overline{R}\right)$, $\overline{R} < 25$ mm, $25 \leq \overline{R} < 50$ mm and $\overline{R} \geq 50$ mm correspond to local, regional and whole-area rainstorm processes, respectively. Processes of convective rainstorm are accompanied by short-time heavy rainfall or thunder and lightning. According to the above definitions, in the east side of the Helan Mountain, a total of 21 rainstorm processes in 2006–2019 (Table 2) and 10 processes in 1951–2005 are selected.

Firstly, based on the rainstorm data set in the east side of the Helan Mountain, the method of linear tendency estimate is used to statistically analyze the inter-annual, and monthly variations of the rainstorm days, frequency, process, precipitation and rainfall intensity extreme values of different rainfall magnitudes, as well as the diurnal variation of the short-time rainstorm frequency and rainfall intensity extreme values.

Secondly, the correlation analysis is used to analyze the spatial distribution of rainstorm days, short-time rainstorm frequency, precipitation amount and rainfall intensity extreme values of different rainfall magnitudes, as well as the correlation between altitude and (short-time) rainstorm frequency, magnitude and intensity.

Then, the detailed characteristics of the 21 rainstorm processes, such as precipitation nature, duration, magnitude, intensity, range, and concentrated period and region, are further analyzed.

Finally, the inter-annual and monthly variations of the rainstorm days, frequency, process, precipitation amount, and rainfall intensity extreme values of different rainfall magnitudes in 1951–2005 are statistically analyzed and compared with the rainfall processes in 2006–2019.

Through above analyses, the influence of ground-based intensified observation and topography on spatio-temporal distribution of rainstorms in the study area, the regional characteristics of rainstorms in

Table 2
Rainstorm processes in the east side of the Helan Mountain from 2006 to 2019.

Rainstorm period	Duration/ h	Average rainfall/ mm	Rainstorm frequency	Short-time rainstorm frequency	Lightning frequency	Lightning intensity / KA(Time)	Maximum cumulative rainfall/ mm	Maximum hour rainfall intensity/ mm (time)	Maximum 5 min rainfall intensity/ mm	P_{1h}	F
1100 BJT 14 Jul–1000 BJT 15 Jul 2006	23	78.7	14	16	yes		168.2	★33.3(0000)	11.4	0.34	0.72
1300 BJT 16 Jun–1200 BJT 17 Jun 2007	24	58.1	14		2	115.0 (1300)	93.5	16.6(0800)	5.1	0.2	0.39
0800 BJT 7 Jul–0700 BJT 8 Jul 2009	24	22.6	10	8	14	−122.2 (1600)	107.6	39.6(2200)	5.2	0.36	0.47
2000 BJT 29 Jul–1100 BJT 30 Jul 2012	16	59.8	52	21	440	−196.0 (2200)	174.3	★47.7(0000)	15	0.37	0.55
0400 BJT 3 Sept–0100 BJT 4 Sept 2015	21	18	11	1			65.9	★27.9(0700)	15.5	0.6	0.33
0100–2000 BJT 8 Sept 2015	20	23	5	3			69.6	★50.4(1000)	8.6	0.77	0.46
0500–1200 BJT 24 Jul 2016	8	25.1	8	20	9	65.2 (0500)	89.5	56.5(0700)	8.3	0.72	0.38
1500 BJT 13 Aug–1400 BJT 14 Aug 2016	24	13.5	32	48	136	216.0 (1700)	110.2	★51.7(1800)	12.4	0.73	0.67
1900 BJT 21 Aug–0800 BJT 22 Aug 2016	14	6.6	10	28	265	−216.4 (0100)	241.7	82.5(0100)	16.6	0.86	0.72
2200 BJT 22 Aug–0600 BJT 23 Aug 2016	9	6.7	3	14	20	−152.8 (0300)	57.3	★53.7(0400)	5.9	0.99	0.34
1500 BJT 4 Jun–1000 BJT 5 Jun 2017	20	37.9	121	4			116.5	26.7(2300)	8	0.36	0.55
0300–1800 BJT 5 Jul 2017	16	10.9	10	17	65	107.5 (0300)	114.4	47.4(1300)	9.7	0.71	0.34
2000 BJT 25 Jul–0200 BJT 26 Jul 2017	6	4.7	4	35	4	−77.3 (2200)	64.4	★57.7(2200)	14.3	0.94	0.27
0900 BJT 1 Jul–0100 BJT 2 Jul 2018	17	19.5	38	24			84.3	★29.8(2000)	9.5	0.51	0.47
0300–1000 BJT 19 Jul 2018	8	8.7	21	39	115	−124.9 (0300)	136.2	★54.5(0500)	9.4	0.65	0.51
1900 BJT 22 July–0700 BJT 23 Jul 2018	13	11.7	35	61	1820	177.4 (0000)	277.6	74.1(0200)	18.7	0.5	0.83
1200–2000 BJT 23 Jul 2018	9	19.4	21	95	101	159.7 (1400)	89.3	★58(1600)	15.5	0.82	0.46
1200 BJT 6 Aug–1600 BJT 7 Aug 2018	29	14.7	18	51	396	−151.8 (1500)	119.1	★51(1700)	16.3	0.52	0.47
1200 BJT 9 Aug–1300 BJT 10 Aug 2018	26	13.4	14	29	911	−218.2 (1100)	71.4	71.4(1300)	12.1	1	0.42

(*continued on next page*)

Table 2 (*continued*)

Rainstorm period	Duration/ h	Average rainfall/ mm	Rainstorm frequency	Short-time rainstorm frequency	Lightning frequency	Lightning intensity / KA(Time)	Maximum cumulative rainfall/ mm	Maximum hour rainfall intensity/ mm (time)	Maximum 5 min rainfall intensity/ mm	P_{1h}	F
1900 BJT 31 Aug–1700 BJT 1 Sept 2018	23	22.8	60	53	5	52.4 (2300)	136.9	★65.1(0100)	8.7	0.64	0.71
1800 BJT 2 Aug–0000 BJT 3 Aug 2019	7	9.8	6	35	60	168.6 (1900)	71	53.9(2100)	8.5	0.98	0.41

Note: all precipitation statistics in the table include all stations throughout the study area; ★ indicates that the center of rainstorm is not consistent with the maximum rainfall intensity.

arid areas, the variation trend of rainstorm magnitude and intensity could be better understood under the background of global warming.

2.3. Preliminary exploration of the joint effect of low-level jet and topography on the distribution of rainstorms

In the past 30 years, several observational experiments have been carried out to investigate the dynamic and thermal effects of topography on precipitation (Houze et al., 2017; Smith et al., 2012; Xu and Chen, 2006; Rotunno and Houze, 2007; Neiman et al., 2002). The results show that the synoptic and mesoscale environments generally favorable for the formation of orographic precipitation include strong LLJ, strong unsteady airflow passing mountains, steep terrain and a quasi-stationary weather system (Lin et al., 2001; Sinclair et al., 1997; Hobbs, 1975; Bergeron, 1960). The researches of Colle (2004), Ralph et al. (2004, 2005), Galewsky and Sobel (2005) and Veals et al. (2018) also showed that under the complex terrain conditions, the increasing effect of LLJ on precipitation is mainly reflected in the enhancement of moisture convergence and uplifting trigger mechanism in front of the windward slope, which reduces the atmospheric stability and is conducive to the occurrence and development of mesoscale convective systems in front of mountain. Tao (1980), Qian et al. (2018) and Chen et al. (2020) pointed out that the rainstorm in the east of Northwest China is closely related to the LLJ, and the rainstorm center usually appears on the windward slope. Therefore, in this paper, the typical rainstorm processes are selected. Then, the ERA-Interim daily reanalysis data, radar data and 5-min surface precipitation are used to investigate the joint effect of LLJ and topography on rainstorms in the Helan Mountain area.

To date, no unified standard on LLJ has been formed due to the differences in the altitude, range, wind speed intensity and wind shear of LLJs in different regions. Referring to past studies (Bonner, 1968; Stensrud, 1996; Higgins et al., 1997; Tao, 1980; Chen et al., 2005; Vera et al., 2006; Pham et al., 2008; Du et al., 2012; Rijo et al., 2018), in our study the LLJ is identified if the following conditions are satisfied. First, in 30–40°N and 100–120°E, the easterly or southerly wind belt is of a wind speed larger than 10 m/s at 850 hPa or 12 m/s at 700 hPa. Second, its length and width should be larger than 100 km and 10 km, respectively. Third, the vertical wind shear in the jet zone should be more than 2/s, or the wind speed larger than 10 m/s below the height of 3 km could be detected in radar products. When the distance between the rainstorm area and the LLJ axis does not exceed four latitudes (longitudes), it is judged that there are some relations between the LLJ and rainstorm.

According to the above analyses, the distribution characteristics of rainstorm in the study area and the influence mechanism of LLJ and topography on the rainstorm distribution are summarized. The detailed analyses are given in the following section.

3. Spatio-temporal distribution of rainstorms in the east side of the Helan Mountain

3.1. Temporal variations

3.1.1. Inter-annual variations

As shown in Table 3, there are 56 rainstorm days (4 days per year), 479 station times with rainstorm (34.2 station times per year), 21 times rainstorm processes (1.5 times per year), and 1031 station times with short-time rainstorm (73.6 station times per year) during 2006–2019. Specifically, there are 46 GR days (3.2 days per year), 8 HR days (0.5 day per year), and 2 ER days (0.1 day per year). There are 431 station times with GR (30.7 station times per year), 43 station times with HR (3 station times per year), and 5 station times with ER (0.1 station time per year). 10 times GR processes (0.7 time per year), 9 times HR processes (0.6 time per year) and 2 times ER processes (0.1 time per year) are found in the study period. There are 917 station times with GSR (65.5 station times per year), 101 station times with HSR (7.2 station times per year) and 13 station times with ESR (0.9 station time per year). Overall, it can be seen that the rainstorm in the east side of the Helan Mountain is mainly of small magnitude, but the rainstorm process with large rainfall amount is more (accounting for 52% of the total).

In the past 14 years, for all the rainfall magnitudes the rainstorm

Table 3
Comparison of rainfall characteristics in the east side of the Helan Mountain between 2006 and 2019 and 1951–2005.

Characteristic quantity of Rainstorm		2006–2019		1951–2005	
		Quantity	Trend estimate value/ 10a	Quantity	Trend estimate value/ 10a
Rainstorm day	GR	46d	4.3d* *	37d	−0.04
	HR	8d	1.0d* * *	3d	
	ER	2d		0d	
	Total	56d	5.1d* *	40d	−0.06
Rainstorm frequency	GR	431	68.6*	80	−0.06
	HR	43	64.1*	3	
	ER	5	27.3	0	
	Total	479	68.6*	83	−0.08
Rainstorm process	GR	10	0.6	7	
	HR	9	1.2* *	3	
	ER	2		0	
	Total	21	2.4*	10	−0.01
Short-time rainstorm	GSR	917	149.1*		
	HSR	101	16.7*		
	ESR	13	2.1		
	Total	1302	149.1*		
Extreme value of daily rainfall		291.6 mm	75.7 mm	132.9	−0.7 mm
Extreme value of hour rainfall intensity		82.9 mm	25.4 mm*		

Note: *, * * and * * * indicate passing the significance tests of $\alpha = 0.05$, $\alpha = 0.01$ and $\alpha = 0.001$, respectively.

days (Fig. 3a), frequency (Fig. 3b), processes (Fig. 3c), extreme values of daily rainfall and hourly rainfall (Fig. 3d), as well as the frequency of short-time rainstorms (Fig. 3e) have all increased. Except for the ER, ESR and the extreme values of daily rainfall, the increasing trends of other characteristic quantities have all passed the significance test. The greater the rainfall and rainfall intensity are, the more significant the increasing trend is. Every 10 years, the rainstorm days, frequency and processes of all the rainstorm events have increased by 5.1 days, 68.6 station times and 2.4 times, respectively. Similarly, the rainstorm days, frequency and processes of GR events have increased by 4.3 days, 68.6

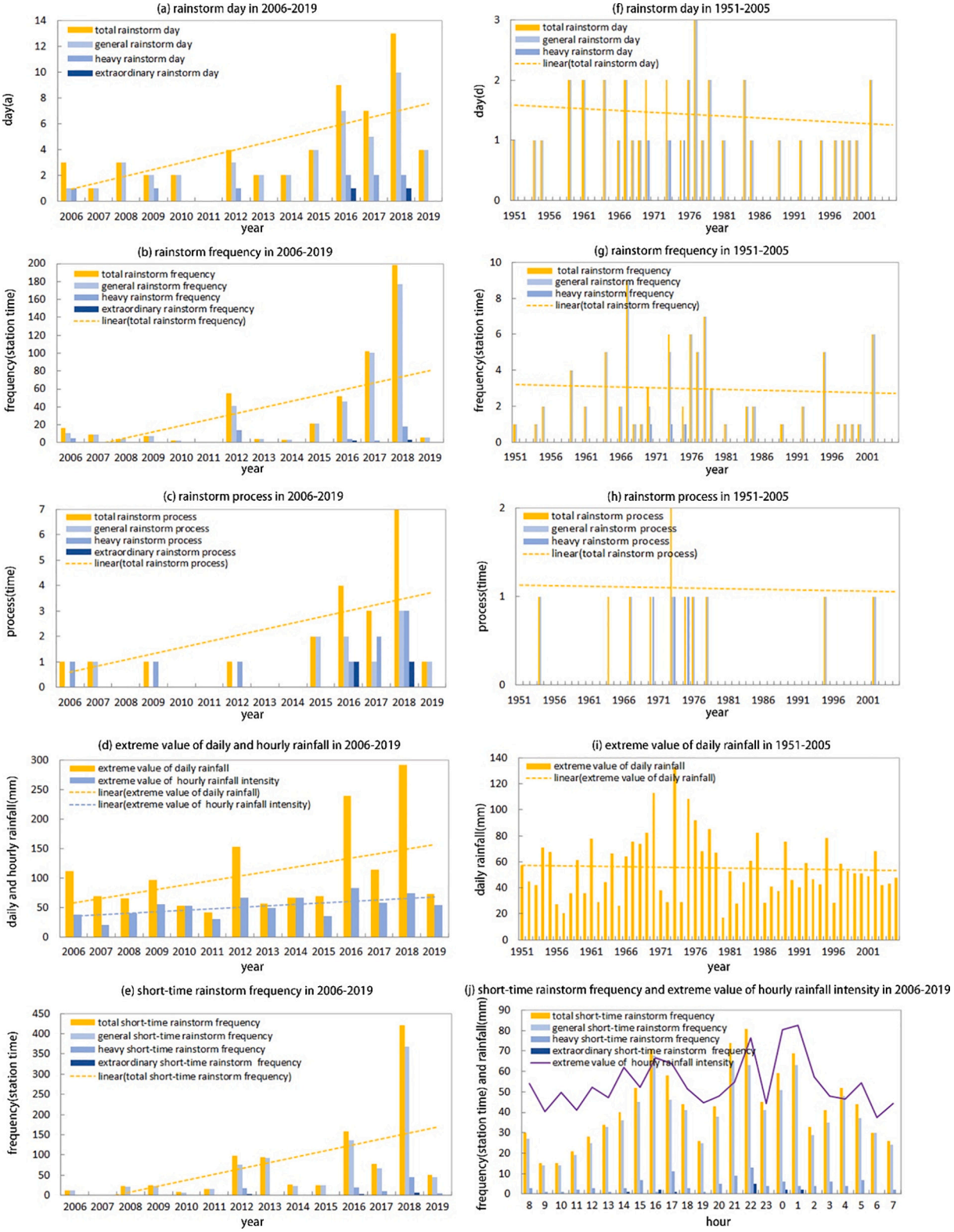

Fig. 3. Comparison of rainstorm days (unit of a and f: day), frequencies (unit of b and g: station time), processes (unit of c and h: time), extreme values (unit of d and i: mm), the inter-annual (unit of e: station time) and daily variations (unit of j: station times) f short-time rainstorm in the east side of the Helan Mountain between (a–e and j) 2006–2019 and (f–i) 1951–2005.

station times and 0.6 time, respectively. The rainstorm days, frequency and processes of HR events have increased by 1.0 day, 64.1 station times and 1.2 times, respectively. The frequency of ER has increased by 27.3 station times. The total frequency of short-time rainstorm, GSR, HSR and ESR has increased by 149.1, 149.1, 16.7 and 2.1 station times, respectively. The extreme values of daily rainfall and hourly rainfall have increased by 75.7 mm and 25.4 mm, respectively. In 2006–2014 and 2019, the rainstorm is relatively few. The rainstorm days, rainstorm frequency and rainstorm processes are mostly below 4 days, 20 station times and 1 time, respectively. In 2015–2018, the rainstorm outbreaks, the days, frequency and processes of rainstorms are above 4 days, 20 station times and 2 times each year. Specially among them, the days, frequency and processes of HR are more than 2 days, 2 station times and 2 times in each year from 2016 to 2018. Besides, in 2016 and 2018, there is one ER event at 2–3 station times. The extreme value of daily rainfall has broken the historical record for four times: 112.1 mm in 2006, 152.9 mm in 2012, 239.1 mm in 2016 and 291.6 mm in 2018, respectively. Before 2015, except 2007, the total frequency of short-time rainstorm larger than 40 station times appears only in 2012 and 2013. In the next four years (2016–2019), the total frequency of short-time rainstorm is all more than 45 station times, which even reaches 137 and 369 station times in 2016 and 2018, respectively. For short-time rainstorm of different magnitudes, when the rainfall intensity is larger, the frequency is lower, and the occurrence years are more concentrated. Specifically, ESR only appears in 4 years (2012, 2014, 2016 and 2018), and the corresponding extreme values of rainfall intensity are 66.7 mm, 66.6 mm, 82.5 mm and 74.1 mm, respectively. The updating frequency of rainstorm extreme-value historical record has been accelerated from 6 years to 2 years.

3.1.2. Monthly and seasonal variations

The days and frequency of rainstorm in the east side of the Helan Mountain appear from late May to early September (Fig. 4a and b), and the rainstorm processes appear from early June to early September (Fig. 4c). The main concentration period of rainstorm is July, and the rainstorm days, frequency and processes account for about 50% of the total. Among them, the rainstorm days are the most in mid July (10 d) and the least in late May and June (1 d). The frequency of rainstorm is the largest in late of July (141 station times) and the least in late May (1 station time). The rainstorm process is the most in late July (5 times), and there are no rainstorm processes in late June. The days and frequency of GR are consistent with the distribution of the total amount of rainstorm, and the GR process has the maximum of 3 times in late July, followed by twice in early both August and September. HR is concentrated in early and mid July (2 d). The frequency of HR has the maximum of 22 station times in late July, followed by 8 station times in mid July; there are no HR in late May, mid June and early August. The HR processes are concentrated in early and mid July (2 times), and there are no HR processes in late August. The ER occurs only in late July and August, with the days, frequency and processes being 1 day, 2–3 station times and 1 time, respectively.

The rainstorm is mainly concentrated in July in the east side of the Helan Mountain. However, it cannot be ignored that, from late May to early June, the strong convective weather in the afternoon increases, and at the same time local HR also occur occasionally. In addition, for early September in early autumn, when the convective weather is not over, the continuous rain in autumn follows subsequently. As the continuous rain process is accompanied by rainstorm and even HR, it is also worthy of attention.

3.1.3. Diurnal variation

From the hourly variations of the total frequency of short-time rainstorm, the rainstorm frequency of different magnitudes and the extreme values of hourly rainfall intensity (Fig. 3j), the diurnal variation has significant nocturnal characteristics. The afternoon to the first half of the night is a period of high frequency. The frequency of short-time rainstorm exhibits a type of double peaks, with the primary and secondary peaks at 21: 00–22: 00 and 16: 00–17: 00 (GSR is opposite), respectively. The extreme value of rainfall intensity exhibits a type of single peak, with the peak value at 01: 00. From 09: 00, the frequency of short-time rainstorm gradually increases, reaching the secondary (primary) peak at 16: 00–17: 00, and rapidly decreases in the subsequent 2–3 h, reaching the maximum (secondary) peak at 21: 00–22: 00, and then slowly declines in fluctuations. The extreme value of rainfall intensity slowly increases in the daytime, peaking at 01: 00, and then rapidly decreases. The total frequencies of short-time rainstorm/GSR/HSR/ ESR in the morning (08: 00–14: 00), afternoon (14: 00–20: 00), the first half of the night (20: 00–02: 00) and the second half of the night (02: 00–08: 00) are 153/ 141/ 11/ 1 station times, 294/ 263/ 28/ 3 station times, 361/312/40/9 stations and 223/ 201/ 22/0 station times, respectively. It can be seen that the frequencies of GSR/HSR/ESR at night are 1.3/ 1.3/1.6/2.3 station times more than that in the daytime,

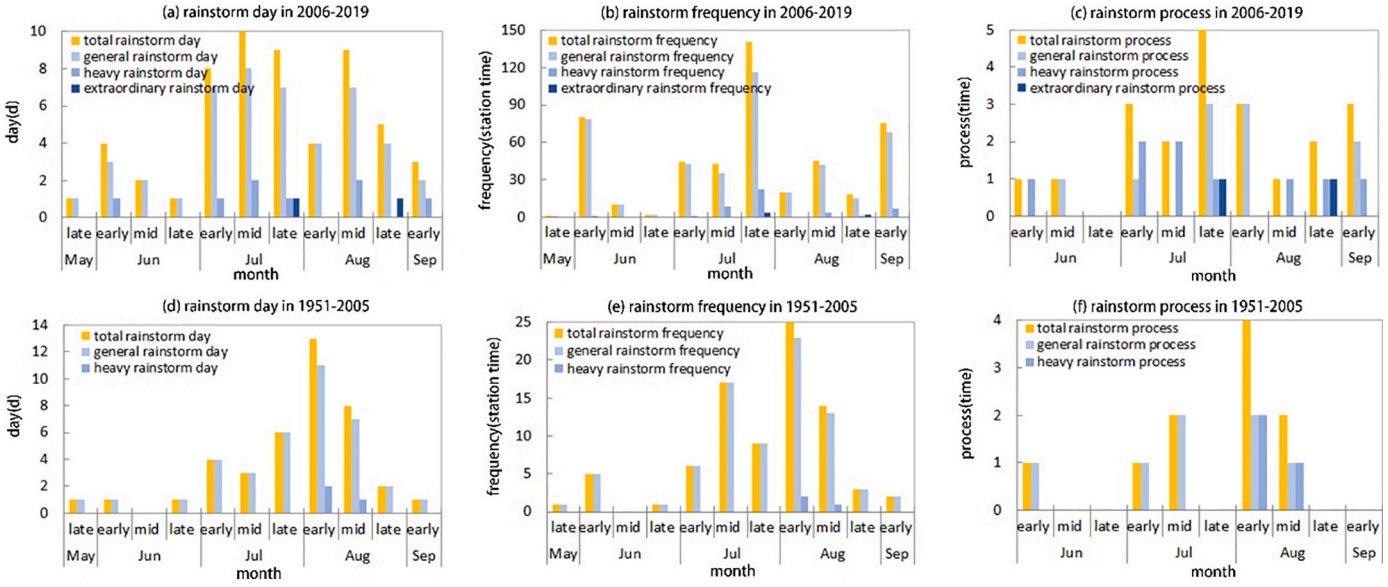

Fig. 4. Comparison of monthly variations of rainstorm days (unit of a and d: day), frequencies (unit of b and e: station time) and processes (unit of c and f: time) in the east side of the Helan Mountain between (a–c) 2006–2019 and (d–f) 1951–2005.

respectively. The greater the rainfall intensity is, the more the times will be. The short-time rainstorm is most likely to occur at the first half of the night, followed by in the afternoon, and the least is in the morning. However, the frequency of ESR has only appeared at 14: 00–17: 00 and 22: 00–01: 00, and the frequency of the latter is 2.5 times larger than that of the former. The top 3 of the extreme values of hourly rainfall intensity, namely 82.5 mm, 80.6 mm and 76.6 mm, appear at 01: 00, 00: 00 and 22: 00, respectively, with all at the first half of the night.

3.2. Spatial distribution

3.2.1. Rainstorm days and short-time rainstorm frequency

Due to a larger proportion of stations in plain areas, the total (short-time) rainstorm, general (short-time) rainstorm and heavy (short-time) rainstorm are mainly distributed in plain areas, and the short-time rainstorm is more widely distributed than the rainstorm days. However, the stations with total rainstorm days ≥6 d, GR days ≥5 d, HR days ≥2 d, frequency of both total rainstorm and GSR ≥ 7 d and frequency of HSR ≥ 2 d are mainly concentrated in mountainous areas, among which the three stations with ER and four stations with ESR are all located in mountainous areas. The greater the magnitude of precipitation is, the lower the days or frequencies, the fewer the stations and the more concentrated the rainfall area will be, indicating a more obvious topography-induced effect (Fig. 5).

3.2.2. Extreme values of rainstorm

There are 237 stations (46%) with the extreme value of daily rainfall ≥50 mm, which appear throughout the region, but are more concentrated in the mountainous areas with larger magnitude. There are 44 stations with extreme value above 100 mm and three stations with extreme value above 200 mm, accounting for 19% and 1% of the number of stations with extreme value above 50 mm, respectively, which mainly appear in mountainous areas, with an average altitude of 1350 mm. The top three extreme values are 291.6 mm for Huaxuechang, 229.9 mm for Yanhua and 225.6 mm for Baisigou, with the altitude of 1494 m, 1443 m and 1384 m, respectively. The stations with the extreme value of daily rainfall of ≥50 mm in the plain areas are relatively scattered, with most stations less than 75 mm (Fig. 6a).

There are 300 stations (58.7%) with the extreme value of hourly rainfall intensity of ≥20 mm, scattered throughout the region, but with larger magnitude and more concentrated in the mountainous area. The areas with the extreme value of ≥40 mm/h are concentrated in the mountainous areas, while the areas with the extreme value above 60 mm/h are only in the mountainous areas, with an average altitude of 1237 m. The top three are 82.5 mm/h for Huaxuechang, 80.6 mm/h for Baisigou and 66.9 mm/h for Mingchangcheng (with an average altitude of 1272 m). There are also stations with extreme values ≥40 mm/h in the plains, distributing dispersedly with a smaller range, with the extreme values at most stations below 40 mm/h (Fig. 6c).

In general, with the increase of altitude, the number of rainstorm days increases, the magnitude and intensity increases and the region with rainstorm is more concentrated, but the correlation is not obvious across all study areas. The correlation coefficients of the altitude with the number of rainstorm days (Fig. 7a), the frequency of short-time rainstorm (Fig. 7b), the daily rainfall (Fig. 7c) and the extreme value of hourly rainfall intensity (Fig. 7d) are 0.1, 0.09, 0.06 and 0.01, respectively. The altitude corresponding to the large-value centers of these four quantities is 1385 m, 1337/ 1827/ 2421 m, 1494 m and 1494 m, respectively. Only in the range of 1200–494 m, for an increase of every 100 m in altitude, the daily rainfall and hourly rainfall intensity

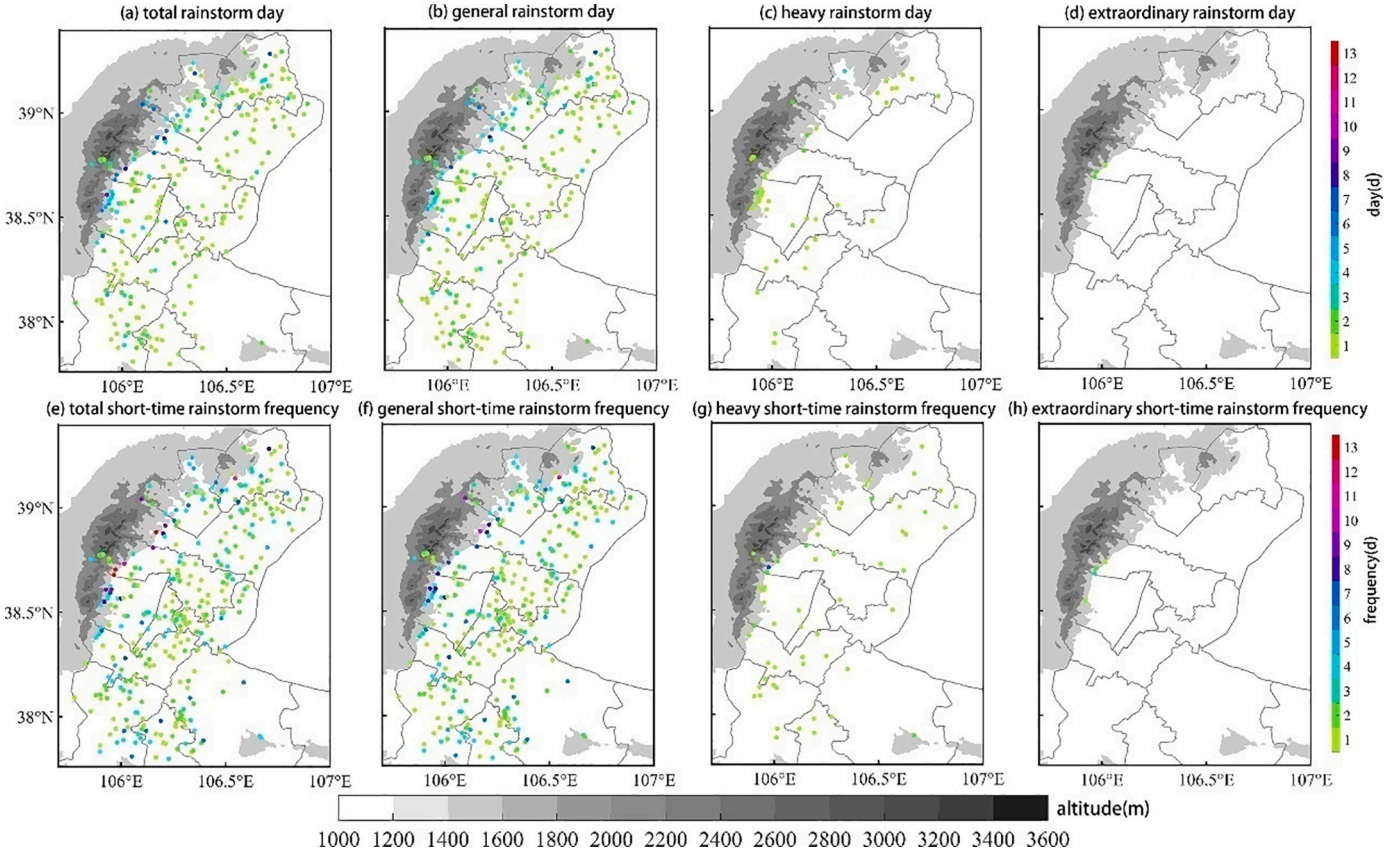

Fig. 5. Distributions of (a–d) rainstorm days and (e–h) frequencies of short-time rainstorm in the east side of the Helan Mountain during 2006–2019 (unit: d; red dots indicate the centers of heavy precipitation). Figs. a–d represent total rainstorm, general rainstorm, heavy rainstorm and extraordinary rainstorm, respectively. Figs. e–h represent total short-time rainstorm, general short-time rainstorm, heavy short-time rainstorm and extraordinary short-time rainstorm, respectively. The colored dots represent the number of days or frequencies of the station.

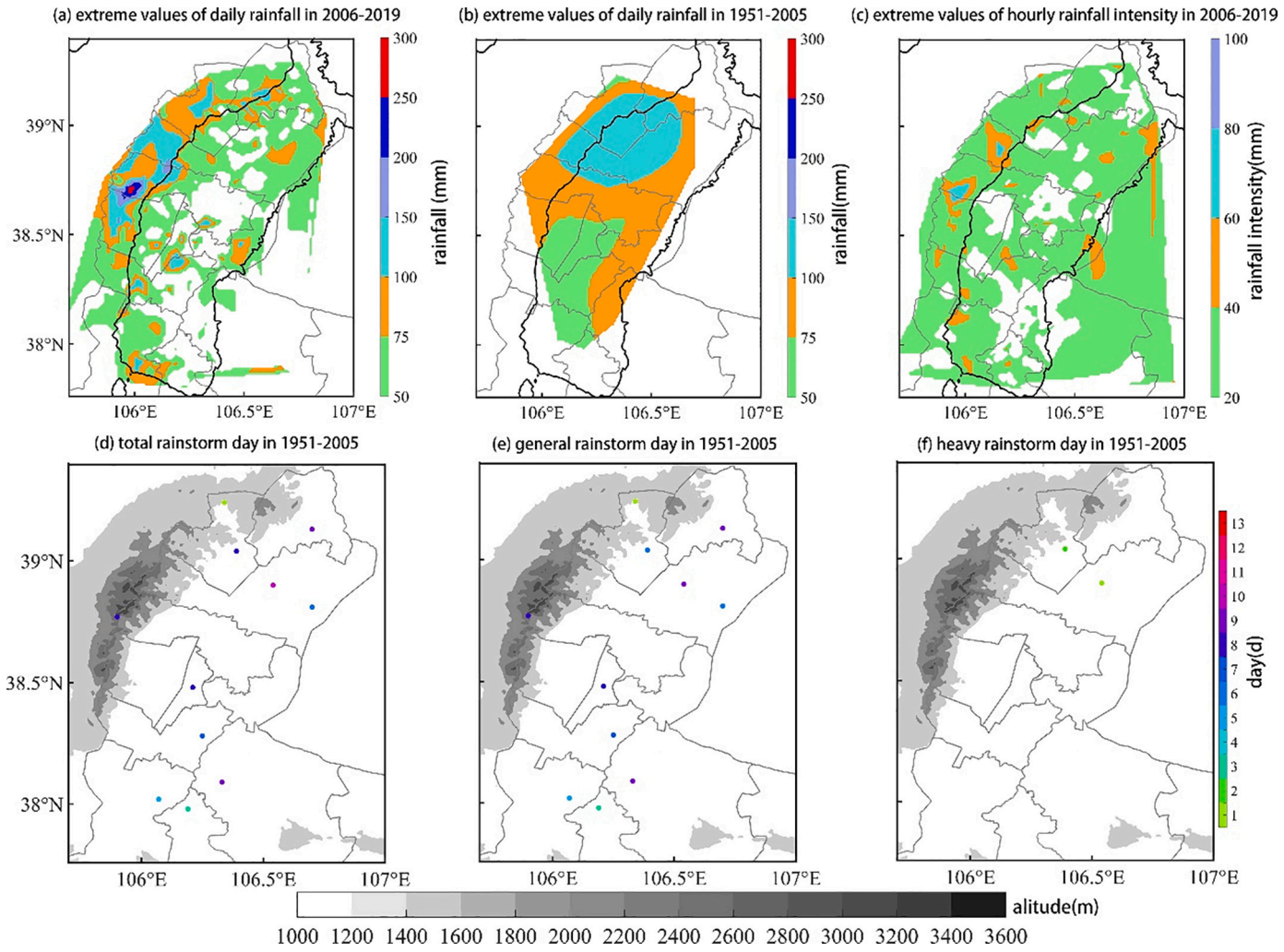

Fig. 6. Distributions of extreme values of daily rainfall (a) and hourly rainfall intensity (c) from 2006 to 2019; distribution of extreme values of daily rainfall (b) and rainstorm days (d–f) from 1951 to 2005 in the east side of the Helan Mountain (unit of rainfall and rainfall intensity: mm; unit of rainstorm days: day). Figs. d–f represent total rainstorm, general rainstorm and heavy rainstorm, respectively. The gray shadow indicates the altitude (unit: m). The colored dots represent the number of days of the station.

would increase by about 21 mm and 5 mm, respectively, with relatively obvious correspondences.

3.3. Characteristics of precipitation distribution during rainstorm process

The fine distribution characteristics of the precipitation in the rainstorm process in the east side of the Helan Mountain are further analyzed from the perspective of the magnitude, intensity, precipitation efficiency, concentration period and region, as well as extreme value change (Table 2).

(1) Severe convection generally occur during the rainstorm processes. There are 20 processes accompanied by the short-time rainstorm (95%), 17 processes by the thunder and lightning (81%), 16 processes by both (76%), and all processes are accompanied by either short-time rainstorm or thunder and lightning. For most of the processes with the frequency of thunder and lightning over 100 times, the frequency of rainstorm (short-time rainstorm) is ≥20 (30) stations, the maximum R_{1h} is ≥50 mm, and the maximum R_{5min} is ≥12 mm; while for most of the processes without thunder and lightning, the frequency of short-time rainstorm is <4 stations, R_{1h} is <30 mm and R_{5min} is <10 mm. It can be seen that the higher the frequency and intensity of thunder and lightning are, the higher the frequency and intensity of rainstorm and short-time rainstorm are, and the greater the rainfall intensity will be. The maximum intensity of thunder and lightning in most processes occur 1–2 h ahead of the maximum rain intensity.

(2) The processes in the study area are dominated by long duration rainstorm. There are 15 processes with durations ≥10 h (71%), among which the durations of 10 processes are ≥20 h (48%), but there are only 6 processes with durations ≤10 h (29%). The study area is dominated by long duration rainstorm.

(3) The precipitation during the rainstorm process is also characterized by large magnitude, strong intensity and high precipitation efficiency. The number of the process with the total rainfall of $R_{24}' \geq 100$ mm is more than half of the total; 20 processes are with $F > 0.33$, of which 8 processes are with $F > 0.5$, with the maximum of 0.83 (occurring on July 22, 2018, 18.7.22 for short, the same below); 13 processes are with $R_{1h} \geq 50$ mm and $P \geq 0.6$, 9 processes with $R_{5min} \geq 10$ mm. Fig. 7e–h shows that 50–99% of the total rainfall is concentrated within 4 h. For two ER processes (occurring on July 22, 2018 and August 21, 2016), the R_{24}' are 277.6 mm and 241.7 mm, respectively; R_{1h} are 71.4 mm and 82.5 mm, respectively; R_{5min} are 16.6 mm and 18.7 mm, respectively; the 4-h rainfall accounts for more than 80% of R_{24}'. It can be seen

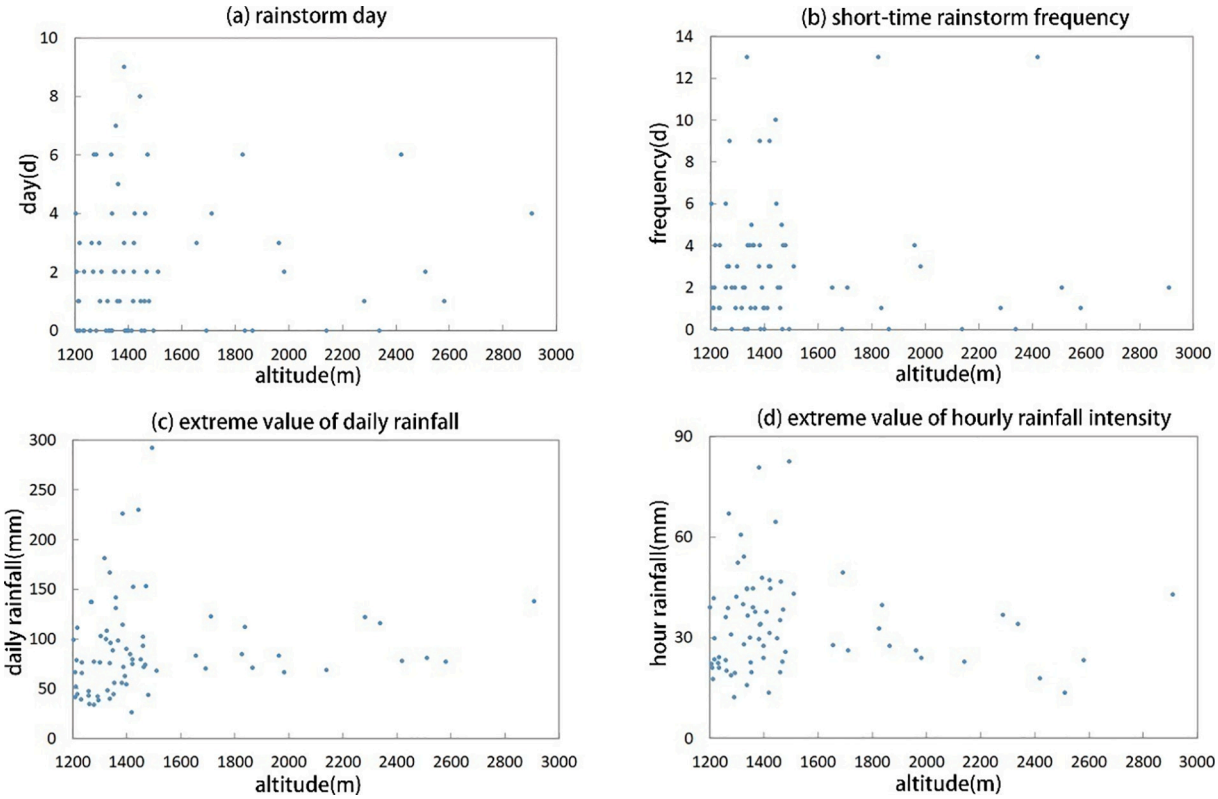

Fig. 7. Variations of (a) rainstorm day, (b) short-time rainstorm frequency, extreme value of (c) daily rainfall and (d) hourly rainfall intensity with the altitude (unit: m) from 2006 to 2019 in the east side of the Helan Mountain (unit of rainstorm day and frequency: day; unit of rainfall and rainfall intensity: mm).

that in the east side of the Helan mountainous areas although the rainstorm processes are characterized by long durations, the short-time rainstorm accounts for the most, and the precipitation during 1–2 HR processes mainly contributes to the annual precipitation of most stations.

(4) Local and topographical features are prominent with the rainstorm processes. There are 16 local (76%), 2 regional (24%) and 3 whole-area (14%) rainstorm processes, with the maximum regional average rainfall of 78.7 mm (occurring on July 14, 2006) and the minimum regional average rainfall of 4.7 mm (occurring on July 25, 2017); among them, 2 ER and 4 HR processes are classified as local rainstorm, and 5 HR processes as regional or whole-area rainstorm. The rainfall distribution during the rainstorm processes (Figs. 1a and 8a–d) reveals that the rainstorm areas and centers of the whole-area, most local and partial regional processes are distributed in mountainous areas, accounting for 71% of the total processes; the centers of both HR and ER are in mountainous areas, with an average altitude of 1407 m. The rainstorm centers are mostly concentrated at the station of the Huaxuechang, with 2 ER and 1 HR. It can be seen that the east side of the Helan Mountain is dominated by local rainstorm, with the rainstorm areas and centers mainly concentrated in mountainous areas.

(5) The rainstorm tends to peak at night. There are 13 rainstorm processes with the heavy rainfall concentrating during the night (62%), when the peak rainfall intensities of 2 ER and 7 HR appear. For 17 processes accompanied by thunder and lightning, severe thunder and lightning of 10 processes occur at night (59%).

(6) Moreover, the frequency of extreme rainstorms has increased in recent years. During 2016–2019, the number of HR processes and the number of stations with short-time rainstorm are 2 times and 11 times more than those before 2016, respectively; the features of rainstorm such as the number of stations with HR, the rainfall at the rainstorm center, the maximum 1 h and 5 min rainfall intensity, precipitation efficiency and relative intensity are 1 time larger, and the ER even broke the record of zero; all the extreme values of rainstorm appeared in 2016 and 2018, with the refreshing frequency of extreme values of rainstorm accelerating to 2 years (Fig. 3a–e).

3.4. Comparison of rainstorm characteristics after and before 2006

As shown in Table 3, from 1951 to 2005, there are 40 rainstorm days (0.7 day per year), 83 stations with rainstorm (1.5 station times per year) and 10 rainstorm processes (0.1 time per year) in total in the east side of the Helan Mountain, including 37 GR days (0.6 day per year) and 3 HR days (0.05 day per year); 80 station times with GR (1.4 station times per year) and 3 station times with HR (0.05 station time per year); 7 GR processes (0.1 time per year) and 3 HR processes (0.05 time per year). The rainstorm days, frequency, processes and extreme values of daily rainfall with different magnitudes show weak decreasing trend, and do not change significantly. The historical record of extreme rainstorm occurred at Pingluo in 1970 (113.2 mm) and at Dawukou in 1973 (132.9 mm) (Fig. 3f–i), with both the rainfall area, center, extreme rainstorm in the plain areas (Figs. 2b, 6b and d–f). The rainstorm is mainly concentrated in August, with high incidence in early August, and the rainstorm processes end in the middle August (Fig. 4d–f).

Compared with the decreasing trend in previous 55 years (1951–2005), since 2006, the increasing trend in recent 14 years is more significantly. The concentration period of rainstorm is one month ahead and the end of the process has been delayed by 20 days (Fig. 4). The annual average rainstorm days, rainstorm process, rainstorm frequency and the maximum daily rainfall have increased by 5.6, 7.5, 22.8 and 2.7 times, respectively. The days, processes and frequencies of GR and HR have increased by 4.9/ 7/ 21.9 times and 12.8/ 2/ 60 times,

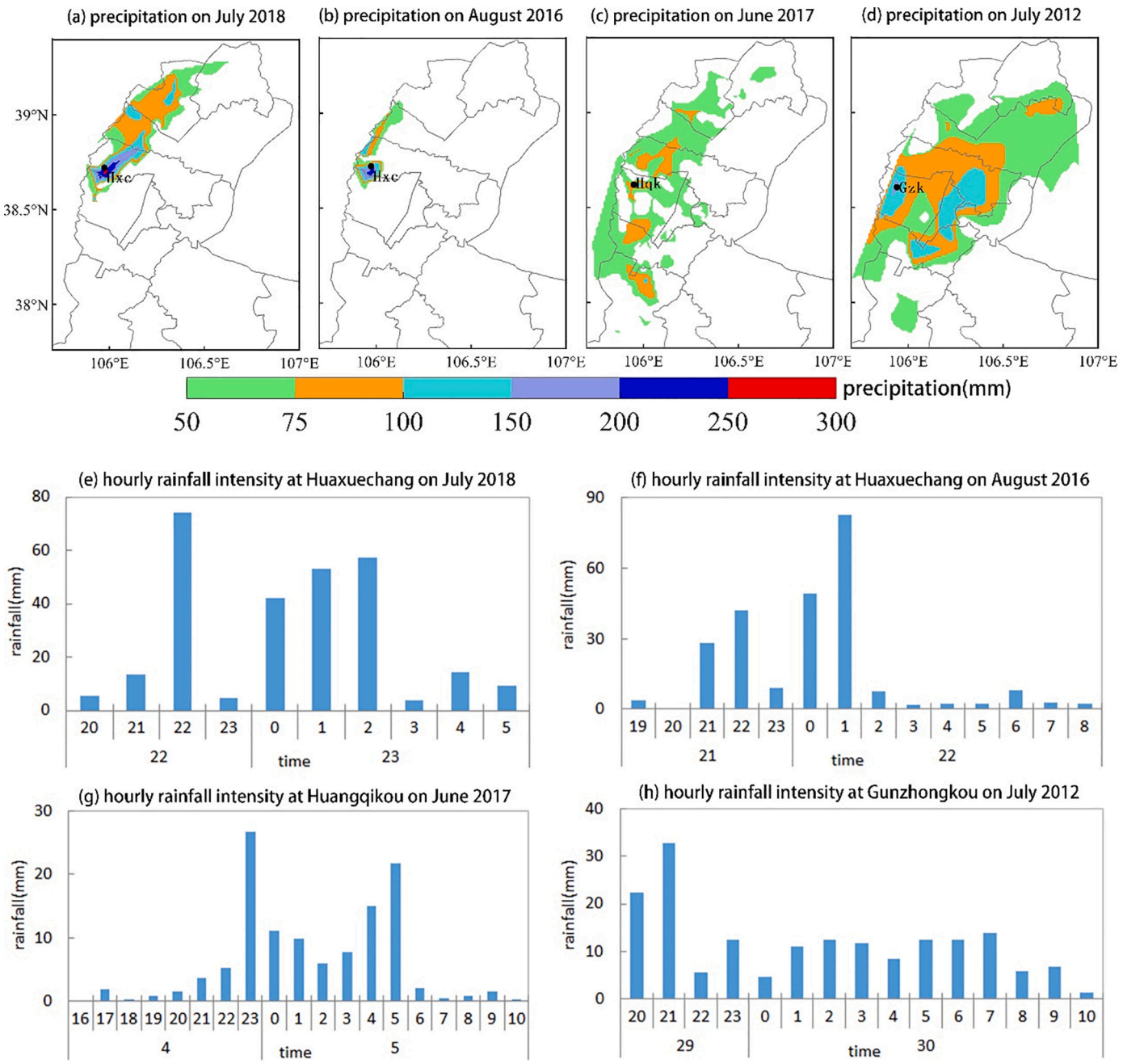

Fig. 8. Distribution of cumulative precipitation and the variation of hourly rainfall intensity at the rainstorm centers of typical rainstorm processes in the east side of the Helan Mountain (unit: mm; black dots indicate rainstorm centers) at Huaxuechang (hxc) (a and e) from 19:00 on July 22 to 05:00 on July 23, 2018 and (b and f) from 19:00 on August 21 to 08:00 on August 22, 2016; (c and g) at Huangqikou (hqk) from 16:00 on June 4 to 10:00 on June 5, 2017; (d and h) at Gunzhongkou (gzk) from 20:00 on July 29 to 10:00 on July 30, 2012.

respectively; the increase times of HR is 2–3 times that of GR; moreover, the ER not only create a breakthrough of the zero record, but also set the historical record for two consecutive times in just three year (Fig. 3). Compared with the previous rainstorm distribution based on national stations, which cannot reflect the effect of the topography of the Helan Mountain on rainstorm, the rainstorm area and center in recent 14 years are mainly distributed in mountainous areas, with all the rainstorm centers located in regional stations, thereby the influence of topography, distribution and number of stations on rainstorm is clearly depicted (Figs. 5–6).

The above analyses show that in the context of global warming, with the improvement of observation technology and data refinement, we have found more mesoscale information of rainstorm in the east side of the Helan Mountain. The rainstorms are more frequent and intense, and the extremity is more severe. Besides, the influence of topography on rainstorm distribution is more clearly presented. Then in the following, aimed at the concentration period, area and magnitude of rainstorms, which are the focus and difficulty of rainstorm forecast, we discuss the joint impact of LLJ and topography on rainstorm distribution.

4. Preliminary exploration of the impact of the combination of low-level jet and topography on the distribution of rainstorm

The above analysis shows that the topography has an important influence on the distribution of precipitation. The topography has a significant effect on the increase of precipitation, and rainstorm always

occurs at night. LLJ is the key weather system because the topography is constant and it needs to interact with other physical quantities. Previous studies have shown that the nighttime enhancement of the rainstorm in front of the windward slope is closely related to the super-geostrophic characteristics of the LLJ, the cyclonic convergence caused by the forced lifting of the airflow in front of the windward slope, and the vertical momentum transport caused by the thermodynamic effect of the atmosphere. These key factors could provide sufficient vapor, strong instability energy and favorable triggering conditions for the nighttime development of the mesoscale rainstorm systems (Hovmoller, 1949; Rudari et al., 2004; Qian et al., 2004; Tucker and Crook, 2005; Chen et al., 2005; Zhang et al., 2006; Zhao, 2012; Wang et al., 2014; Yuan et al., 2014; Li et al., 2017; Chen et al., 2017a, 2017b; Chen et al., 2018; Li et al., 2018; Fu et al., 2019; Pan and chen, 2019; Ivonne and Bollasina, 2020; Zhao et al., 2020).

Statistics show that all 21 rainstorm processes in the east side of the Helan Mountain are accompanied by LLJ. Taking the nighttime rainstorm on July 22, 2018 as an example, the evolution process of the topographic rainstorm enhanced by LLJ in conjunction with topography is preliminarily discussed.

Heavy precipitation was concentrated in front of the east side of the Helan Mountain at the first half of the night on July 22, which is a typical topography-induced localized severe convective rainstorm (Table 2 and Fig. 8a). 6 h before the rainstorm (14: 00–20: 00 on July 22), the LLJ at 700 hPa was established, thereby the warm and humid airflows from the South China Sea, the East China Sea and the Yellow Sea were merged in the Sichuan Basin, which then strengthened and turned northward, forming a water vapor transport channel that passed through the rainstorm area. The increased temperature and humidity in lower layer promoted the reduction of atmospheric stability. During the period of heavy precipitation from 20: 00 on July 22 to 02: 00 on July 23, with the strengthening and northward moving of the LLJ, the area from Sichuan to the central–southern Ningxia was dominated by a strengthened southerly jet with the central wind speed ≥18 m/s (Fig. 9a), which continuously transported the water vapor to the rainstorm area. The rainstorm area was located in the large–value area of water vapor flux and convergence, and there was a region with high temperature and high humidity in mid and low level, and the dense area of the gradient of θ_{se} (potential pseudo-equivalent temperature) isolines formed in the vertical and horizontal directions was the front area where the cold and warm air masses interacted, which was conducive to the development of the atmospheric instability. However, as there was no obvious horizontal wind convergence at low level, the weak synoptic system forced a weak upward movement, of which the center was located at 800 hPa, with the center value of only 0.2 Pa/s (Fig. 9b). Although the effect of dynamic lifting is insufficient, the strong and persistent high

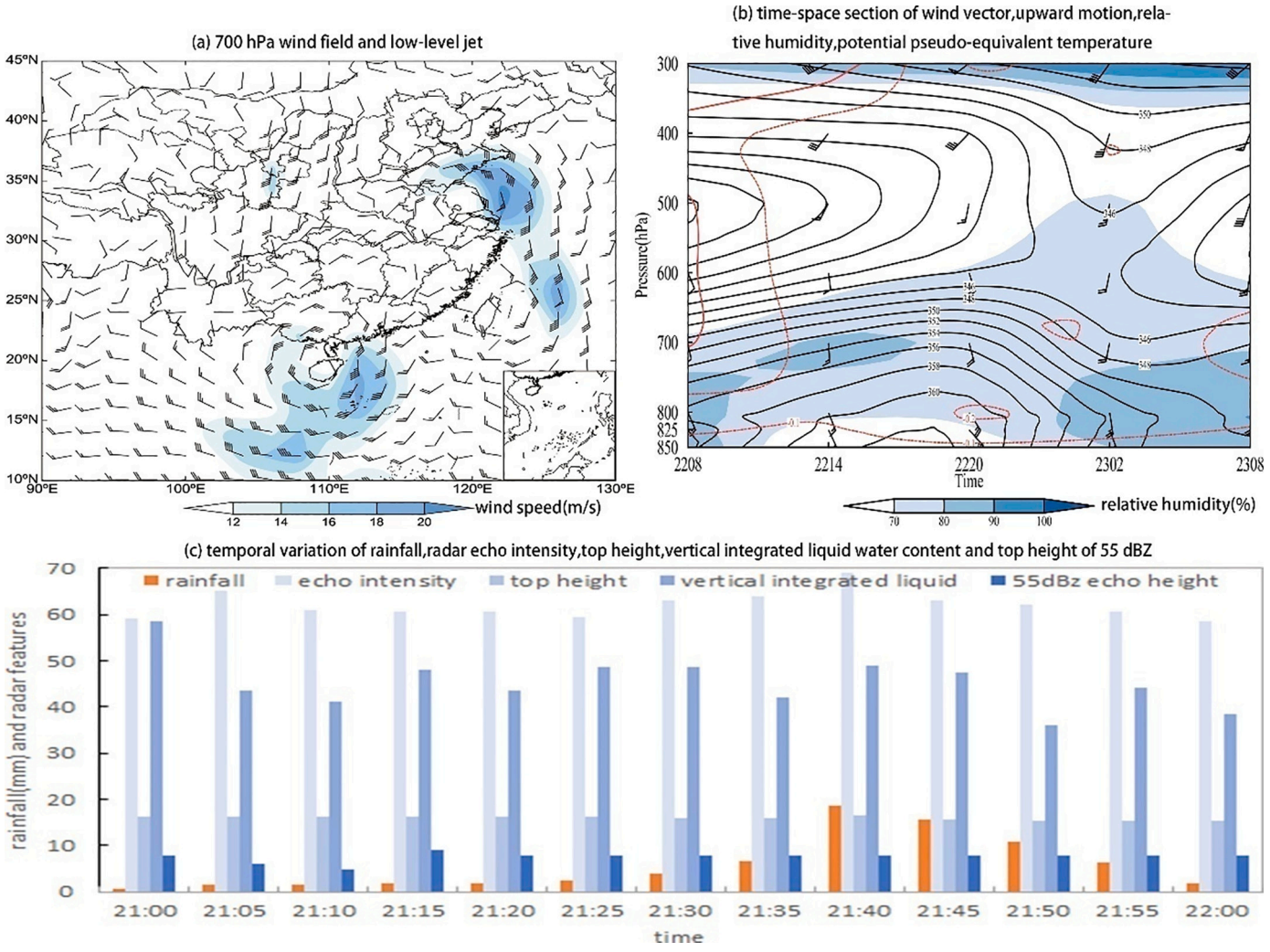

Fig. 9. (a) 700 hPa wind field (unit: m/s) and the low-level jet (shading indicates wind speed ≥12 m/s) at 02:00 on July 23, 2018; (b) time-space section of wind vector, upward motion (dashed line; unit: hPa/s), relative humidity ≥70% (shadow) and potential pseudo-equivalent temperature (black solid line; unit: K) at the rainstorm center of ski resort (105.9°E, 38.7°N) at the night on July 22; (c) temporal variations of 5-min rainfall (unit: mm), radar echo intensity (unit: dBZ), echo top height (unit: km) and vertical integrated liquid water content (unit: g/kg) and the echo top height of 55 dBZ (unit: km).

temperature and high humidity at low level provided important thermodynamic conditions for triggering the mesoscale convective system. The orographic lifting formed by the combination of the LLJ and the topography of the Helan Mountain was also an important mechanism for triggering the mesoscale convective system related to rainstorm. The monitoring from Yinchuan radar shows that during the strongest period of rainstorm from 21: 00 to 22: 00, the southeastern LLJ reached its strongest development and maintained. The jet core (23.5 m/s) was located about 0.8 km above the radar, and about 15 km southeast away from the radar (Fig. 10a–d). The LLJ moved west to the front of the mountain, and a number of convective cells triggered by orographic lifting propagated along the mountain and moved northward slowly. When passing through the center of the rainstorm, the convective cells were strengthened, forming a cyclonic convergence with stability and less movement (Fig. 10e–h). The hourly average echo intensity near the rainstorm center was 61 dBZ with the top height of 16 km, the liquid water content was 45 kg/g, and the strong echo above 55 dBZ was at the height of about 7.6 km (Fig. 9c), resulting in the heavy rainfall of 74.1 mm/h in the Huaxuechang of rainstorm center (Fig. 8e).

Similar evolutions can also be found during other rainstorm processes accompanied by LLJ. In general, the LLJ is generally established 6–12 h before the rainstorm, and a water vapor transport channel, which is formed by the low-level (easterly) southerly warm-wet air flow at 700 hPa or (and) 850 hPa from the eastern or (and) southern ocean, passes through the rainstorm area. The LLJ starts from the Sichuan basin, which is also the place for the gathering and transferring of water vapor; at night, the LLJ enhances and moves northward or westward, with the front of the jet axis moving toward the eastern slope of the Helan Mountain. The warming and humidifying of the rainstorm area at low-level, the increase of the atmospheric instability, and the enhancement of the dynamic or (and) thermal as well as the orographic lifting conditions, provide favorable environmental conditions for the triggering and developing of the mesoscale convection system related to the rainstorm. The rainstorm area is mostly found on the left front of the LLJ axis; when the LLJ is the strongest and the LLJ axis is the closest to the rainstorm area, the precipitation is the strongest; the closer the LLJ axis moves northward or westward to the east slope of the Helan Mountain and the larger the LLJ core is, the stronger the magnitude and the intensity of the rainstorm will be.

5. Conclusions and discussion

By using high-resolution rainstorm data sets, the distribution and variation characteristics of the rainstorm in the east side of the Helan Mountain in China from 2006 to 2019 are statistically analyzed, and the comparison with those in 1951–2005 has also been conducted. Moreover, the influences of the interaction between LLJ and topography on the distribution of rainstorm are preliminarily explored. The conclusions are as follows.

(1) The rainstorm in arid areas is characterized by distinctive geographical characteristics, including small scope, high

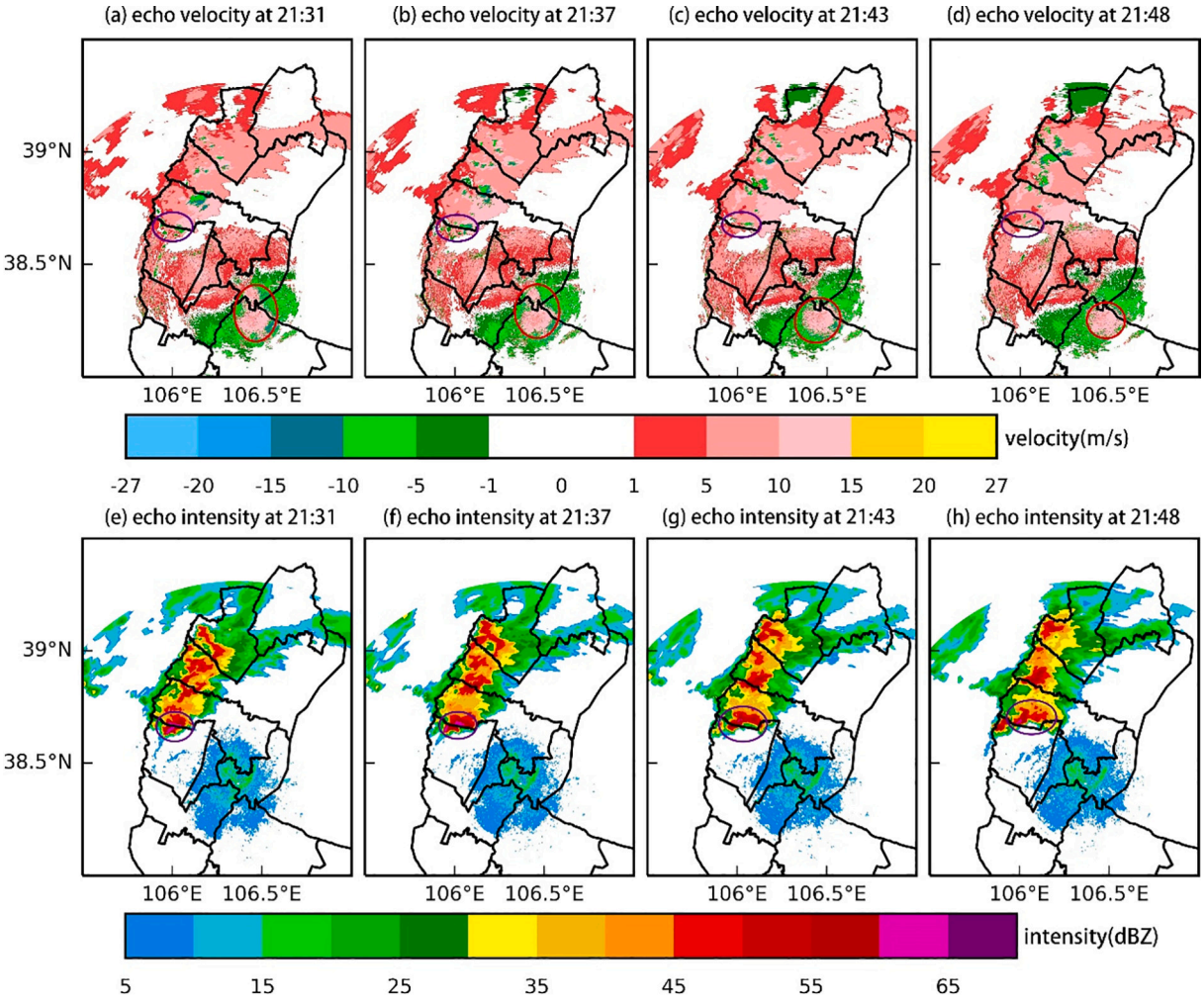

Fig. 10. (a–d) Echo reflectivity (unit: dBZ) and (e–h) velocity (unit: m/s) at the elevation angle of 2.4° of Yinchuan radar at (a, e) 21:31, (b, f) 21:37, (c, g) 21:43 and (d, h) 21:48 on July 22, 2018 (purple circles indicate the mesoscale systems near the rainstorm center, and red circles indicate the low-level jet cores).

intensity, short duration for heavy rainfall, strong localization, high precipitation efficiency and obvious topographic features, with significant night peaks. The process is often accompanied by LLJ, short-time rainstorm or (and) thunder and lightning. Such precipitation distribution is closely related to the increase of topography induced precipitation caused by the nighttime enhancement of the low-level southeastern jets and the combination with the topographic influence in front of the east side of the Helan Mountain that triggers or enhances the meso- and micro-scale systems related to rainstorm.

(2) In general, the frequency and magnitude of rainstorms are smaller in our study area than those in other regions. The annual average for the days and frequency of GR are 3.2 days and 30.7 station times, while that for the days of both HR and ER is less than 1 day, but the processes account for 52%. Compared with 1951–2005, during 2006–2019 the annual average of rainstorm days, processes, frequencies and the extreme value of daily rainfall have increased by 5.6 times, 7.5 times, 22.8 times and 2.7 times, respectively, and the greater the rainfall and rainfall intensity are, the more obvious the increase will be; the increase of the days and frequency of HR is 2–3 times more than that of the GR; ER has not only created a breakthrough of the zero record, but also refreshed the historical record for two consecutive times in just 3 years. The more frequent and intense rainstorm and the severer extremity are related to the global climate warming and the intense observation data used in this study.

(3) The days and frequencies of rainstorm appear from the last ten days of May to the first ten days of September, and the rainstorm processes occur from the first ten days of June to the first ten days of September, with July being the concentration period and the last ten days of July being the peak period. The days of GR are concentrated in the middle ten days of July, while the frequency and process aappear in the last ten days of July; the days and processes of HR are concentrated in the first and middle ten days of July, with the frequencies in the last ten days of July; the ER has only occurred in the last ten days of both July and August. During 2006–2019, the concentration period of rainstorm is one month ahead and the end of the rainstorm process is delayed by 20 days compared with those before 2006. The monthly and seasonal variations of rainstorms in arid areas are closely related to the position of the ridge line of the western Pacific tropical high. From the middle ten days of June to the last ten days of August, as the ridge line of the western Pacific tropical high jumps to about 30°N, the rainy season of North China begins.

(4) The short-time rainstorm has significant diurnal variations with significant night peaks, showing a distribution of double peaks for the frequency and a distribution of single peak for the extreme values, with the high-frequency occurrence appearing from the afternoon to the first half of the night. The stronger the rainfall intensity is, the more? the times will be; the first half of the night has the most, followed by the afternoon, and the least is in the morning; the primary and secondary peaks occur at 21: 00–22: 00 and 16: 00–17: 00, respectively (which is opposite for GSR), while ESR only appears at 14: 00–17: 00 and 22: 00–01: 00, and the frequency of the latter is 2.5 times more than that of the former; the top three extreme values of rainfall intensity all appear in the first half of the night. The nocturnal occurrence of rainstorm is related to the enhancement of the LLJ supergeostrophic characteristics (Tao, 1980).

(5) The high-frequency, high-value areas and the centers of the rainstorm are mainly located in mountainous areas. In general, as the altitude increases, the frequency, magnitude and intensity of rainstorm increase. Within the range of 1200–1494 m, the daily rainfall and hourly rain intensity increase by about 21 mm and 5 mm for every increase of 100 m in the altitude. The rainstorm distribution in plain areas is relatively more scattered, with lower frequency and smaller magnitude. At most stations, the total frequency of rainstorms is below 3 days, the extreme daily rainfall is less than 75 mm, and the extreme hourly rainfall intensity is less than 40 mm. The topography has important influence on rainstorms, and the rainstorm frequency and rainfall intensity are more frequent and intense in mountain areas.

The influence of the LLJ combined with the topography on the distribution of rainstorm is preliminarily explored. Considering the paper length limit, only the observational facts are detailedly presented, but the reasons behind the facts are just preliminarily analyzed. The triggering mechanisms of rainstorms over complex terrain still need further investigation. In future researches, based on high-resolution numerical simulation and sensitivity test on typical rainstorm processes, the triggering, developing and dissipation mechanisms for the rainstorm-related mesoscale systems over complex terrains will be thoroughly explored, aiming to figure out the formation mechanisms of the rainstorm in the east side of the Helan Mountain.

Declaration of Competing Interest

We declare that we have no financial and personal relationships with other people or organizations that can inappropriately influence our work, there is no professional or other personal interest of any nature or kind in any product, service and/or company that could be construed as influencing the position presented in, or the review of, the manuscript entitled, “Spatio-temporal distribution of the rainstorm in the east side of the Helan Mountain and the possible causes of its variability”.

Acknowledgments

This study was supported by the National Natural Science Foundation of China (41965001).

References

Bai, Z.Y., Xu, G.C., Sun, X.J., 1988. Weather in Northwest China. Meteor. Press, BeiJing, pp. 250–254.
Ban, N., Schmidli, J., Schaer, C., 2014. Evaluation of the convection-resolving regional climate modeling approach in decade-long simulations. J. Geophys. Res. Atmos. 119, 7889–7907.
Bergeron, T., 1960. Operation and results of “Project PluviuS”. Phys. Precipitation. 5, 152–157.
Bonner, W.D., 1968. Climatology of the low level jet. Mon. Weather Rev. 96, 833–850.
Chen, Y., Zhai, P.M., 2013. Persistent extreme precipitation events in China during 1951–2010. Clim. Res. 57, 143–155.
Chen, T.J., Wang, C.C., Lin, T.W., 2005. Characteristics of low-level jets over northern Taiwan in mei-yu season and their relationship to heavy rain events. Mon. Weather Rev. 133, 20–43.
Chen, X.G., Declan, C., Chen, X.J., Zheng, G.F., 2008. Trend analysis of extreme precipitation events in Ningxia from 1961 to 2005. Adv. Clim. Chang. Res. 4, 156–160.
Chen, Y.N., Deng, H.J., Li, B.F., Li, Z., Xu, C.C., 2014. Abrupt change of temperature and precipitation extremes in the arid region of Northwest China. Quat. Int. 336, 35–43.
Chen, G.X., Lan, R.Y., Zeng, W.X., Pan, H., Li, W.B., 2017a. Diurnal variations of rainfall in surface and satellite observations at the monsoon coast (South China). J. Clim. 31, 1703–1724.
Chen, G.X., Sha, W.M., Iwasaki, T., Wen, Z.P., 2017b. Diurnal cycle of a heavy rainfall corridor over East Asia. Mon. Weather Rev. 145, 3365–3389.
Chen, Y.Y., Chen, N., Ren, X.F., Wang, Y., 2018. Analysis on forecast deviation and predictability of a rare severe rainstorm along the Eastern Helan Mountain. Meteorol. 44, 159–169 (in Chinese with English abstract).
Chen, Y.Y., Su, Y., Yang, Y., Zhang, S.Z., Yang, J., 2020. The Mesoscale Characteristics of Extreme Rainstorm in the Eastern Region of Helan Mountain. Plateau. Meteor (doi: 10. 7522/j. issn. 1000–0534. 2020. 00012).
China, M. A, 2012. GB/T 28592–2012 Grade of Precipitation. China Quality and Standards Publishing & Media Co., Ltd., Beijing.
Colle, B.A., 2004. Sensitivity of orographic precipitation to changing ambient conditions and terrain geometries: an idealized modelling perspective. J. Atmos. Sci. 61, 588–606.
Deng, H.J., Chen, Y.N., Shi, X., Li, W.H., Wang, H.J., Zhang, S.H., Fang, G.H., 2014. Dynamics of temperature and precipitation extremes and their spatial variation in the arid region of Northwest China. Atmos. Res. 138, 346–355.

Ding, Y.H., Ren, G.Y., Zhao, Z.C., Xu, Y., Luo, Y., Li, Q.P., Zhang, J., 2007. Detection causes and projection of climate change over China: an overview of recent progress. Adv. Atmos. Sci. 24, 954–971.
Du, Y., Qing, H.Z., Yue, Y., Yang, Y.M., 2012. Characteristics of low-level jets in Shanghai during the 2008–2009 warm seasons as inferred from wind profiler radar data. J. Meteor. Soc. Jpn. 90, 891–903.
Fischer, E.M., Knutti, R., 2015. Anthropogenic contribution to global occurrence of heavy-precipitation and high-temperature extremes. Nat. Clim. Chang. 5, 560–564.
Fu, P.L., Zhu, K.F., Zhao, K., Zhou, B.W., Xue, M., 2019. Role of the nocturnal low-level jet in the formation of the morning precipitation peak over the Dabie Mountains. Adv. Atmos. Sci. 36, 15–28.
Galewsky, J., Sobel, A., 2005. Moist dynamics and orographic precipitation in northern and Central California during the New Year's flood of 1997. Mon. Weather Rev. 133, 1594–1612.
Hanel, M., Buishand, T.A., 2010. On the value of hourly precipitation extremes in regional climate model simulations. J. Hydrol. 393, 265–273.
Higgins, R.W., Yao, Y., Yarosh, E.S., Janowiak, J.E., Mo, K.C., 1997. Influence of the great plains low-level jet on summertime precipitation and moisture transport over the Central United States. J. Clim. 10, 481–507.
Hobbs, P.V., 1975. The nature of winter clouds and precipitation in the Cascade Mountains and their modification by artificial seeding. Part I: Natural condition. J. Appl. Meteorol. 14, 783–804.
Houze, R.A., McMurdie, L.A., Petersen, W.A., Schwaller, Mathew R., Baccus, William, Lundquist, Jessica, Mass, Cliff, Nijssen, Bart, Rutledge, Steven A., Hudak, David, Tanelli, Simone, Mace, Gerald G., Poellot, Michael, Lettenmaier, Dennis, Zagrodnik, Joseph, Rowe, Angela, DeHart, Jennifer, Madaus, Luke, Barnes, Hannah, 2017. The olympic mountains experiment(OLYMPEX). Bull. Am. Meteor. Soc. 98, 2167–2188.
Hovmoller, E., 1949. The trough and ridge diagram. Tellus. 1, 62–66.
IPCC, 2013. Intergovernmental Panel on Climate Change: Fifth Assessment Report (AR5). Cambridge University Press, Cambridge, UK (2216pp).
Ivonne, M. García-Martínez, Bollasina, M.A., 2020. Sub-monthly evolution of the Caribbean Low-Level Jet and its relationship with regional precipitation and atmospheric circulation. Clim. Dyn. https://doi.org/10.1007/s00382-020-05237-y in press.
Jing, C., Tong, J., Wang, T.J., Chen, J., Jian, D.N., Luo, L.X., Su, B.D., 2016. A study on regional extreme precipitation events and the exposure of population and economy in China. Acta. Meteorol. Sin. 74, 572–582.
Johnson, R., Mapes, B.E., 2003. Meso-scale processes and severe weather. Chapter 3. In: Emanuel, D.V. Parson L., Enitch, J.M., Weisman, M., Zhang, D.L. (Eds.), Severe Local Storms, 28. American Meteor. Society. Meteor Monographs.
Jung, I.W., Bae, D.H., Kim, G., 2011. Recent trends of mean and extreme precipitation in Korea. Int. J. Climatol. 31, 359–370.
Li, Z.Q., Niu, F., Fan, J.W., Daniel, R., Ding, Y.N., 2011. Long-term impacts of aerosols on the vertical development of clouds and precipitation. Nat. Geosci. 4, 888–894.
Li, B.F., Chen, Y.N., Shi, X., Chen, Z.S., Li, W.H., 2013. Temperature and precipitation changes in different environments in the arid region of Northwest China. Theor. Appl. Climatol. 112, 589–596.
Li, J., Chen, T.R., Li, N.N., 2017. Diurnal variation of summer precipitation across the Central Tian Shan Mountains. J. Appl. Meteorol. Climatol. 56, 1537–1550.
Li, P.X., Furtado, K., Zhou, T.J., Chen, H.M., Li, J., Guo, Z., Xiao, C., 2018. The diurnal cycle of East Asian summer monsoon precipitation simulated by the Met Office Unified Model at convection-permitting scales. Clim. Dyn. https://doi.org/10.1007/s00382-018-4368-z.
Lin, Y.L., Chiao, S., Wang, T.A., Kaplan, Michael L., Weglarz, Ronald P., 2001. Some common ingredients for heavy orographic rainfall. Weather Forecast. 16, 633–660.
Neiman, P.J., Ralph, F.M., White, A.B., Kingsmill, D.E., Persson, P.O.G., 2002. The statistical relationship between upslope flow and rainfall in California's coastal mountains: Observations during CALJET. Mon. Weather Rev. 130, 1468–1492.
Nuissier, O., Joly, B., Joly, A., Ducrocq, V., 2011. A statistical downscaling to identify the large-scale circulation patterns associated with heavy precipitation events over southern France. Quart. J. Roy. Meteor. Soc. 137, 1812–1827.
Orsolini, Y.J., Zhang, L., Peters, D.H.W., Fraedrich, Klaus, Liu, X.H., Schneidereit, Andrea, van den Hurk, Bart, 2015. Extreme precipitation events over North China in August 2010 and their link to eastward propagating wave-trains across Eurasia: Observations and monthly forecasting. Quart. J. Roy. Meteor. Soc. 141, 3097–3105.
Pan, H., Chen, G.X., 2019. Diurnal Variations of Precipitation over North China Regulated by the Mountain-plains Solenoid and Boundary-layer Inertial Oscillation. Adv. Atmos. Sci. 36, 863–884.
Pham, N., Nakamura, K., Furuzawa, F.A., Satoh, S., 2008. Characteristics of low level jets over Okinawa in the baiu and post-baiu seasons revealed by wind profiler observations. J. Meteorol. Soc. Jpn. 86, 699–717.
Qian, J.H., Tao, W.K., Lau, K.M., 2004. Mechanisms for torrential rain associated with the mei-yu development during scsmex 1998. Mon. Weather Rev. 132, 3–27.
Qian, Z.A., Cai, Y., Song, M.H., Wu, T.W., Zhou, J.Q., Luan, C., 2018. Review of advances in water vapor transport studies of rainstorm in Northwest China. Plat. Meteorol. 37 (3), 577–590 (in Chinese with English abstract).
Qin, Y.H., Li, B.F., Chen, Z.S., Chen, Y.N., Lian, L.S., 2017. Spatio-temporal variations of nonlinear trends of precipitation over an arid region of Northwest China according to the extreme-point symmetric mode decomposition method. Int. J. Climatol. 38, 2239–2249.
Ralph, F.M., Neiman, P.J., Wick, G.A., 2004. Satellite and CALJET aircraft observations of atmospheric rivers over the eastern North Pacific Ocean during the winter of 1997/98. Mon. Weather Rev. 132, 1721–1745.
Ralph, F.M., Neiman, P.J., Rotunno, R., 2005. Dropsonde observations in low-level jets over the northeastern Pacific Ocean from CALJET-1998 and PACJET-2001: mean vertical-profile and atmospheric-river characteristics. Mon. Weather Rev. 133, 889–910.
Ray, P., 1986. Mesoscale Meteorology and Forecasting. American Meteor. Soc, Boston (793pp).
Rijo, N., Semedo, A., Miranda, P.M.A., Lima, D., Cardoso, R.M., Soares, P.M.M., 2018. Spatial and temporal variability of the Iberian Peninsula coastal low-level jet. Int. J. Climatol. 38, 1605–1622. https://doi.org/10.1002/joc.5303.
Rotunno, R., Houze, R.A., 2007. Lessons on orographic precipitation from the Mesoscale Alpine Programme. Quart. J. Roy. Meteor. Soc. 133, 811–830.
Rudari, R., Entekhabi, D., Roth, G., 2004. Terrain and multiple-scale interactions as factors in generating extreme precipitation events. J. Hydrometeorol. 5, 390–404.
Schmidli, J., Frei, C., 2005. Trends of heavy precipitation and wet and dry spells in Switzerland during the 20th century. Int. J. Climatol. 25, 753–771.
Shao, J., Pei, X.R., Liu, J., Shi, H.L., Wang, S.G., Hu, W.D., 2015. Temporal and spatial distribution characteristics of rainstorms in Ningxia during 1961-2013. J. Arid. Meteor. 33, 595–601.
Shi, Y.F., Shen, Y.P., Kang, E., Li, D.L., Ding, Y.J., Zhang, G.W., Hu, R.J., 2007. Recent and future climate change in Northwest China. Clim. Chang. 80, 379–393.
Sinclair, M.R., Wratt, D.S., Henderson, R.D., 1997. Factors affecting the distribution and spillover of precipitation in the Southern Alps of New Zealand–a case study. J. Appl. Meteorol. 36, 428–442.
Smith, R.B., Minder, J.R., Nugent, A.D., Storelvmo, T., Kirshbaum, D.J., Warren, R., Lareau, N., E Palany, P., James, A., French, J., 2012. Orographic precipitation in the tropics: the dominica experiment. Bull. Am. Meteor. Soc. 93, 1567–1579.
Stensrud, D.J., 1996. Importance of low-level jets to climate: a review. J. Clim. 9, 1698–1711.
Sun, Y.C., Gao, R.N., Gao, N., Cui, Y., Wang, D., 2018. Study on error control technique of rainstorm intensity formula in arid area under the background of climate change. Torrential Rain Disasters. 37, 89–95 (in Chinese with English abstract).
Tao, S.Y., 1977. Some problems associated with the analysis and forecasting of heavy rainfalls. Chin. J. Atmos. Sci. (in Chinese) 1, 64–72.
Tao, S.Y., 1980. Rainstorm of China (in Chinese), 25-32. Science Press, Beijing, pp. 51–64.
Tao, S.Y., Ding, Y.H., 1981. Observational evidence of the influence of the Qinghai-Xizang (Tibet) Plateau on the occurrence of heavy rain and severe convective storms in China. Bull. Am. Met. Soc. 62, 23–30.
Tu, K., Yan, Z.W., Wang, Y., 2011. A spatial cluster analysis of heavy rains in China. Atmos. Oceanic Sci. Lett. 4, 36–40.
Tucker, D.F., Crook, N.A., 2005. Flow over heated terrain. Part II: Generation of convective precipitation. Mon. Weather Rev. l33, 2565–2582.
Veals, P.G., Steenburgh, W.J., Campbell, L.S., 2018. Factors affecting the inland and orographic enhancement of lake-effect precipitation over the Tug Hill Plateau. Mon. Weather Rev. 146, 1745–1762.
Vera, C., Baez, J., Douglas, M., Emmanuel, C., Marengo, J., Meitin, J., Nicolini, M., Paegle, J.N., Paegle, J., Penalba, O., Salio, P., Saulo, A.C., Dias, M.A.F., Dias, P.L.S., Zipser, E.J., 2006. The south American low-level jet experiment. Bull. Am. Meteor. Soc. 87, 63–77.
Wang, J.Z., Yang, Y.Q., Xu, X.D., Zhang, G.Z., 2003. A monitoring study of the 1998 rainstorm along the Yangtze River of China by using TIPEX data. Adv. Atmos. Sci. 20, 425–436.
Wang, C.X., Gao, S.T., Liang, L., Deng, D.F., Gong, H.N., 2014. Multi-scale characteristics of moisture transport during a rainstorm process in North China. Atmos. Res. 145-146, 189–204.
Xu, X.D., Chen, L.S., 2006. Advances of the study on Tibetan Plateau experiment of atmospheric sciences. J. Appl. Meteor. Sci. 17, 756–772.
Xu, J.F., Wang, X.W., 1986. Climatic characteristics of rainstorm in Northwest China. Arid Meteor. 4, 2–5.
Xu, X., Du, Y.G., Tang, J.P., Wang, Y., 2011. Variations of temperature and precipitation extremes in recent two decades over China. Atmos. Res. 101, 0–154.
Xue, J.S., 2005. Some scientific issues on numerical weather prediction in Northeast China. Arid Meteor. 23, 68–71.
Yang, P., Xia, J., Zhang, Y.Y., Hong, S., 2017. Temporal and spatial variations of precipitation in Northwest China during 1960-2013. Atmos. Res. 183, 283–295.
Yao, H.R., Li, D.L., Wang, H., 2017. A comparative analysis of the atmospheric circulation in summertime rainy days with different precipitation intensity in eastern Northwest China during 1981-2012. Acta Meteor. Sin. 75, 384–399.
Yuan, W.H., Sun, W., Chen, H.M., Yu, R.C., 2014. Topographic effects on spatio temporal variations of short-duration rainfall events in warm season of central North China. J. Geophys. Res. 119, 11223–11234.
Zhai, P.M., Zhang, X.B., Wan, H., Pan, X.H., 2005. Trends in total precipitation and frequency of daily precipitation extremes over China. J. Clim. 18, 1096–1108.
Zhang, D.L., Zhang, S.L., Weaver, S.J., 2006. Low-level jets over the mid–Atlantic states: warm-season climatology and a case study. J. Appl. Meteorol. Climatol. 45, 194–209.
Zhang, W., Villarini, G., Vecchi, G.A., Smith, J.A., 2018. Urbanization exacerbated the rainfall and flooding caused by hurricane Harvey in Houston. Nature. 563, 384–388.
Zhao, Y.C., 2012. Numerical investigation of a localized extremely heavy rainfall event in complex topographic area during midsummer. Atmos. Res. 113, 22–39.
Zhao, Y.C., Liu, C.H., Wang, Y.H., Moncrieff, M.W., 2020. Quasi-stationary extreme rain produced by mesoscale convective system on the Mei-Yufront. Meteorog. Atmos. Phys. 1–22. https://doi.org/10.1007/s00703-019-00717-1 inpress.